Holocene surface rupturing earthquakes on the Dinaric Fault System, western Slovenia

Christoph Grützner[1], Simone Aschenbrenner[2,3], Petra Jamšek Rupnik[4], Klaus Reicherter[2], Nour Saifelislam[2], Blaž Vičič[5], Marko Vrabec[6], Julian Welte[1], Kamil Ustaszewski[1]

[1]Institute of Geological Sciences, Friedrich-Schiller-Universität Jena, Jena, 07749, Germany
[2]Neotectonics and Natural Hazards Group, RWTH Aachen University, Aachen, 52056, Germany
[3]Now at: Institute of Geology and Mineralogy, University of Cologne, Cologne, 50674, Germany
[4]Geological Survey of Slovenia, Ljubljana, 1000, Slovenia
[5]The Abdus Salam International Centre for Theoretical Physics, Trieste, 34151, Italy
[6]Department of Geology, University of Ljubljana, Ljubljana, 1000, Slovenia

Correspondence to: Christoph Grützner (christoph.gruetzner@uni-jena.de)

Abstract. The Dinaric Fault System in western Slovenia, consisting of NW-SE trending, right-lateral strike-slip faults, accommodates the northward motion of Adria with respect to Eurasia. These active faults show a clear imprint in the morphology and some of them hosted moderate instrumental earthquakes. However, it is largely unknown if the faults also had strong earthquakes in the Late Quaternary. This hampers our understanding of the regional tectonics and the seismic hazard. Geological evidence of co-seismic surface ruptures only exists for one historical event, the 1511 Idrija Earthquake with a magnitude of ~M6.8, but the causative fault is still disputed. Here we use geomorphological data, near-surface geophysical surveys, and paleoseismological trenching to show that two of these faults, the Predjama Fault and the Idrija Fault ruptured in strong earthquakes in the Holocene. In a paleoseismological trench across the Predjama Fault we found at least one earthquake with a minimum magnitude of $M_W6.1$ that occurred between 13 - 0.7 ka, very likely not earlier than 8.4 ka. At the Idrija Fault, a surface-rupturing earthquake with a magnitude of at least $M_W6.1$ happened in the last ~2.1 ka. This event could correspond to the 1511 Idrija earthquake. Our results show that the faults rupture in rare, but strong earthquakes, which dominate the seismic moment release. We show that instrumental and historical seismicity data do not capture the strongest events in this area. The fact that many of the NW-SE trending, parallel faults are active implies that the deformation in western Slovenia is distributed, rather than focussed on one major structure.

1 Introduction

This paper is concerned with Holocene surface rupturing earthquakes on strike-slip faults belonging to the Dinaric Fault System (DFS) in western Slovenia (Fig. 1). Following the established nomenclature in the literature (e.g., Slejko et al., 1989), the faults are named Dinaric Faults because they strike parallel to the trend of the Dinarides. However, they must not to be confused with the now inactive, SW-vergent Dinaric thrusts. It is well understood that the Dinaric right-lateral faults are active and that they accommodate a share of the relative motion between Adria and Europe (Poljak et al., 2000; Vrabec and Fodor, 2006;

Placer et al., 2010; Moulin et al., 2016; Atanackov et al., 2016). However, so far very little is known about their earthquake record. In this rather slowly deforming region, strong but rare earthquakes may dominate the overall seismic moment release. Identifying the strongest earthquake events in the Late Quaternary will, therefore, help to better understand the regional active

35   tectonics, shed light on the role of individual faults in the deformation of the crust, and better inform seismic hazard assessments.

Regions of slow continental deformation pose a challenge for active tectonics studies for several reasons. (i) In low-strain settings, geodetic techniques that cover only a few decades of monitoring (GPS, InSAR) have to deal with very small amounts of total crustal deformation. This hampers a proper recognition of active structures. (ii) Instrumental seismicity is usually low.

40   Microseismicity studies will, therefore, often not be able to detect active faults. Earthquakes strong enough to compute reliable focal mechanisms, for example by teleseismic body-waveform modelling, may not have occurred during the instrumental era. Thus, our understanding of fault mechanisms and seismogenic faults may be limited. (iii) Large earthquakes are rare. Historical catalogues may contain felt events but do likely not cover the strongest ones the local active faults are capable of because of their long recurrence intervals. Also, historical earthquakes can rarely be tied to their causative faults. Earthquakes strong

45   enough to leave their imprints in the landscape have very large recurrence intervals. Chances are high that their traces were modified or obliterated by erosion and sedimentation before geoscientists started to look out for them at all. Notwithstanding all those issues, studying slowly deforming regions and diffuse plate boundaries is important both from the perspectives of active tectonics (e.g., Stein et al., 2009; Landgraf et al., 2017) and seismic hazard (England and Jackson, 2011).

In our study area at the transition zone between the Eastern Southern Alps and the Dinarides we are confronted with the above-

50   mentioned problems to varying extents. GPS studies show that there is about 3 mm/yr of convergence between Adria and Europe at the longitude of the Eastern Alps (D'Agostino et al., 2005, 2008; Weber et al., 2010; Metois et al., 2015), but the station network is too sparse to assess individual faults. Only few reliable moment tensor solutions are available for moderate earthquakes (Anderson and Jackson, 1987; Herak et al., 1995, Bajc et al., 2001; Pondrelli et al., 2002, 2011; Kastelic et al., 2008) and they did only occur on some of the main faults, for example the Ravne Fault earthquakes in 1998 and 2004 (Fig. 1).

55   For historical earthquakes of M>6 the causative faults are either unknown or debated. Similarly, there is a debate about the strongest historical earthquake on record, the 1511 Idrija earthquake, which may have caused surface ruptures on one or two faults (Fitzko et al., 2005; Bavec et al., 2013; Falcucci et al., 2018).

In this paper we present data from paleoseismological trenches dug across two of the large strike-slip faults in western Slovenia, the Idrija and Predjama Faults. We show evidence for Holocene surface-rupturing earthquakes on those faults and support our

60   interpretation with geomorphological data, geophysical profiling, and radiocarbon dating. We then discuss the implications of our findings in the light of the regional tectonic setting and seismic hazard.

2 Geological and tectonic setting

2.1 Geological background

Our study area is located in western Slovenia in the External Dinarides, close to the transition zone between the eastern

65   Southern Alps and the Dinarides (Fig. 1). The area was shaped by the collision of the Adriatic microplate and Europe during the Cenozoic (Schmid et al., 2008; Placer et al., 2010; Ustaszewski et al., 2010; Handy et al., 2015). Shortening in NE-SW direction and the related SW-directed thrusting of Mesozoic carbonates along NW-SE striking faults lasted from the Cretaceous to the Eocene. From Oligocene to Early Miocene, S-directed transport on E-W striking faults characterised the phase of South Alpine thrusting. Žibret and Vrabec (2016) used paleostress analyses to distinguish three phases of deformation post-dating

70   the late Eocene NE-SW shortening in western Slovenia: Early to Middle Miocene back-arc extension in the Pannonian Basin led to NE-SW extension and normal faulting on NW-SE striking structures. Then, a short pulse of Late Miocene E-W compression led to a left-lateral reactivation of the NW-SE striking faults and N-S extension. Since the Pliocene, N-S shortening is taken up by right-lateral motion on a NW-SE trending strike-slip fault system known as the Dinaric Fault System (e.g. Poljak et al., 2000; Vrabec and Fodor, 2006; Placer et al., 2010; Moulin et al., 2016; Atanackov et al., 2016). This phase

75   lasts until today and is corroborated by seismological data (e.g., Herak et al., 1995; Pondrelli et al., 2002; Vičič et al., 2019), remote sensing and field studies (e.g., Cunnigham et al., 2007; Kastelic et al., 2008; Gosar et al., 2011; Moulin et al., 2014, 2016).

2.2 Active tectonics

The largest faults of the strike-slip Dinaric Fault System in the western part of this system are the Raša, Predjama, Idrija, and

80   Ravne Faults (Figs. 1, 2). The more than 120 km-long Idrija Fault has the most prominent morphological imprint in the study area. It has a total right-lateral offset of around 10 km (Placer et al., 2010) and an almost straight fault trace, pointing to its predominant strike-slip mechanism. Lower offset estimates come from the displacement of the mercury deposits, which were mined in Idrija since more than 500 years (Placer, 1982; Čar, 2010). The first geological evidence for the late Quaternary activity of the Idrija Fault came from faulted fluvial deposits in Kanomlja (Cunnigham et al., 2006; Bavec et al., 2012) and in

85   the Učja River valley (Vrabec, 2012). Geomorphological work showed that the fault offsets the regional drainage system and Late Quaternary morphological markers (Moulin et al., 2014, 2016). Moulin et al. (2016) estimate mean slip rates averaged over the last 255 ka of 1.15 ± 0.15 mm/yr for the Idrija Fault using ^{36}Cl cosmic ray exposure dating. However, short-term slip rates for the Idrija Fault are reported to be as high as 3.8 ± 2.0 mm/yr. Based on the mean slip rates and the total offset, Moulin et al. (2016) concluded that the strike-slip movement on the fault probably originated in the Early Pliocene.

90   The ~75 km long Predjama Fault is estimated to be active since the Middle Pleistocene, based on slip rates from geomorphic offsets and the total amount of slip (Moulin et al., 2016). It parallels the Idrija Fault, but is not as straight and shows a prominent bifurcation at the Čepovan Canyon on the Trnovski Gozd Plateau. Moulin et al. (2016) estimate a slip rate of 1.45 ± 0.25 mm/yr for the Predjama Fault based on offset morphological markers and ^{36}Cl dating.
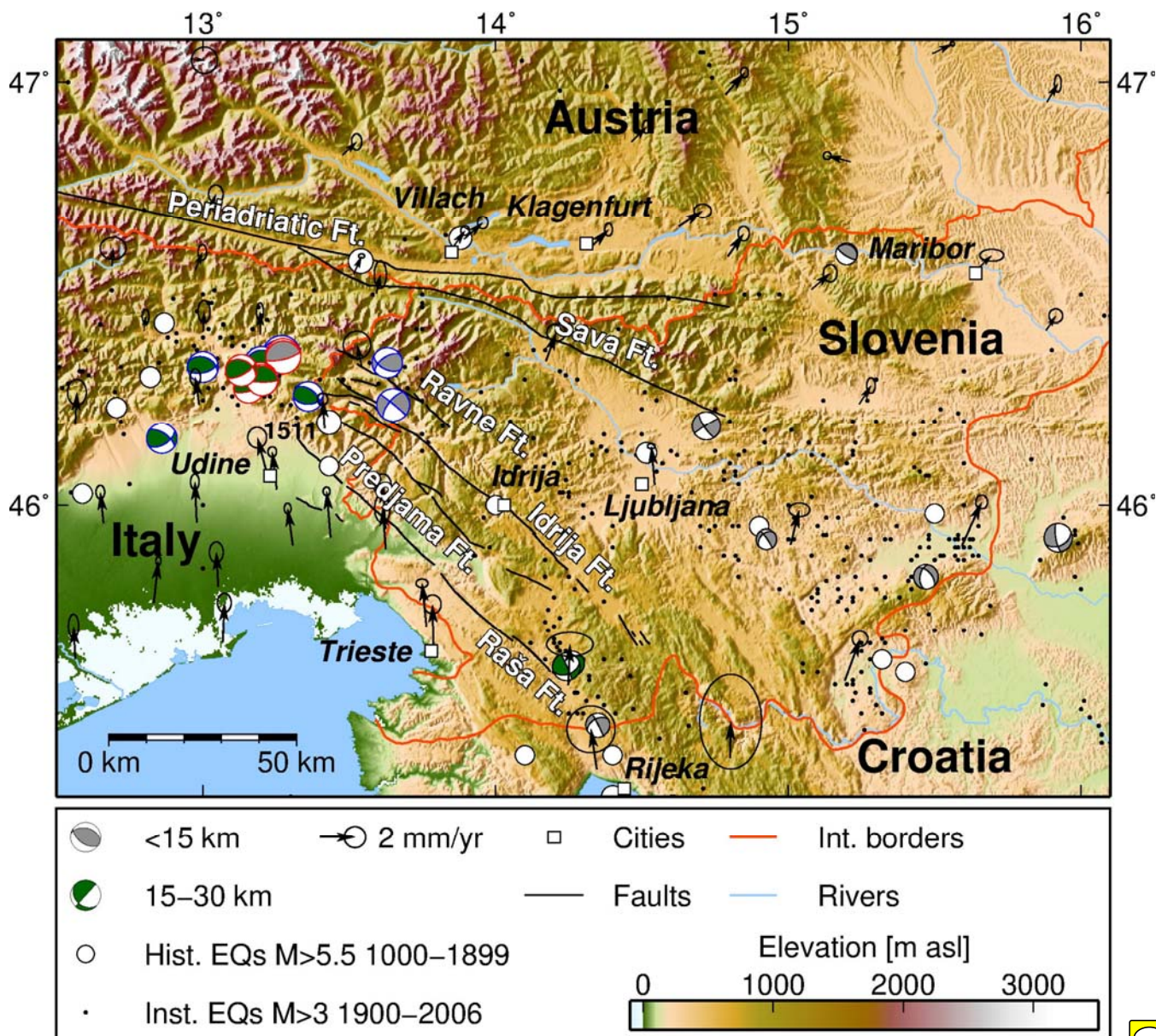
Figure 1: The study area in the Alps-Dinarides transition zone. Main faults of interest (black lines) are from Moulin et al. (2016) and own mapping. Historical and instrumental seismicity are from the SHEEC database (Stucchi et al., 2013; Grünthal et al., 2013); the 1511 Idrija EQ is marked (note that the location is uncertain, the earthquake probably occurred either on the Idrija Fault or on the SW side of the mountain front in Italy). Beachballs with black outlines are derived from p-wave arrivals (Herak et al., 1995); those with blue outlines are from quakes M>5 determined from first arrivals used in the Italian RCMT catalogue 1997-2017 (Pondrelli et al., 2002 and updates thereof); red outlines mark data from teleseismic body waveform inversion 1953-1984 (Anderson and Jackson, 1987). GPS data are from Metois et al. (2015) in a Eurasia-fixed reference frame. Topography is from SRTM1 data.

GPS studies show that there is about 2-3 mm/yr of N-S convergence of Adria vs. Europe at the longitude of the Eastern Alps (D'Agostino et al., 2005, 2008; Weber et al., 2010; Fig. 1) and a counter-clockwise rotation of Adria about an Euler pole in

the Western Alps of not more than 0.52°/Ma (Calais et al., 2002; Weber et al., 2010). This is in line with slip vectors of large
105   earthquakes that occurred around the internally almost aseismic Adriatic Plate (Anderson and Jackson, 1987). As of today, the
published GPS vectors in Slovenia are too coarse to allow for a more detailed analysis of single faults.
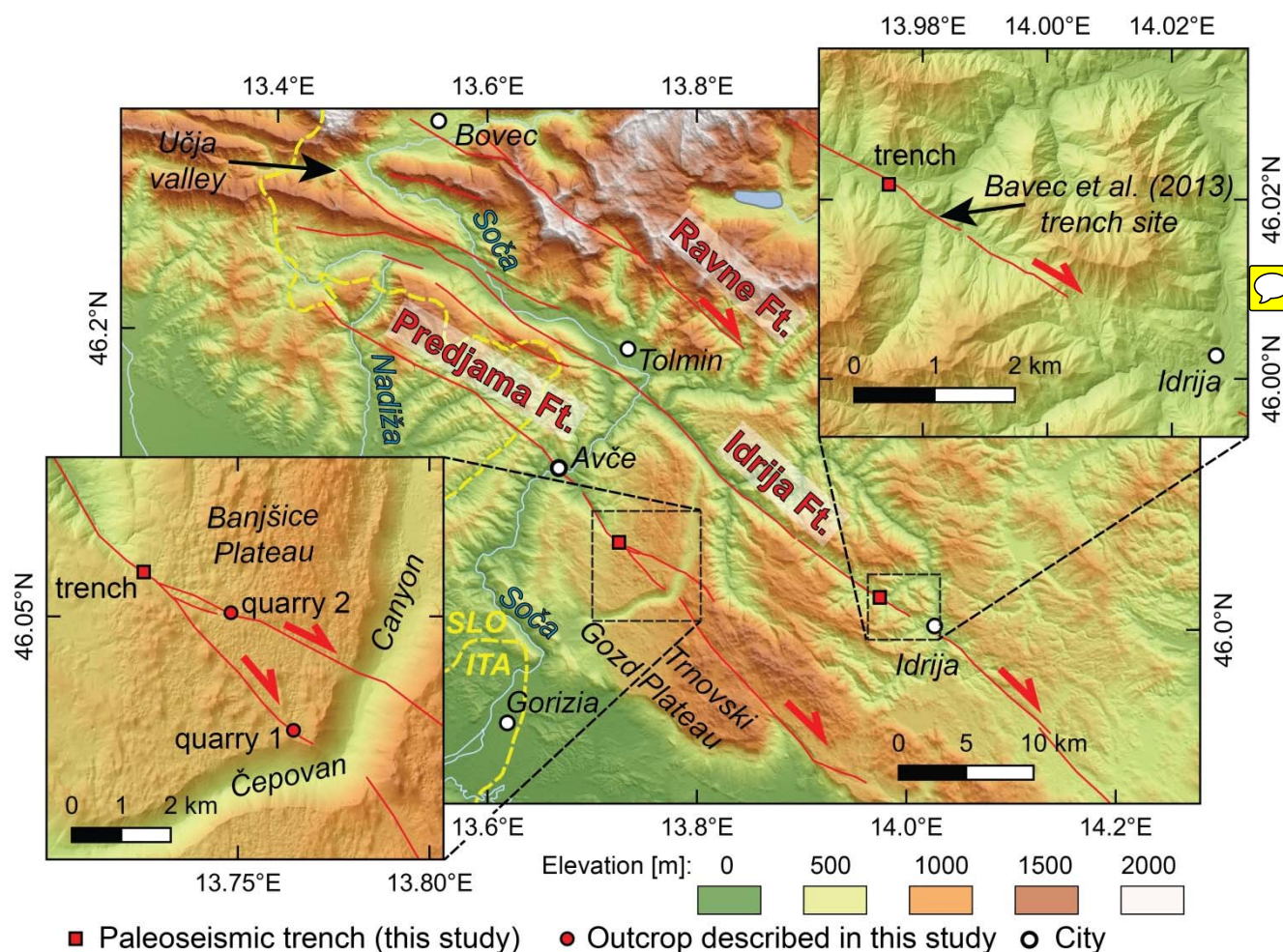
Figure 2: The study sites in NW Slovenia. At the Predjama Fault, we trenched the single strand section of the fault. At the Idrija Fault, the trench site is close to the one of Bavec et al. (2013). Faults are from Moulin et al. (2016) and own mapping.

110   Large instrumental earthquakes with well-constrained fault plane solutions in the study area are rare. The 1976 Friul sequence
occurred on an N-dipping, E-W trending thrust fault (e.g., Aoudia et al., 2000; Peruzza, 2002) at the southern Alpine front.
Two shallow earthquakes of magnitude $M_S5.7$ and $M_W5.2$ occurred on the Ravne fault in 1998 and 2004, respectively (Bajc
et al., 2001; Kastelic et al., 2004, 2008). One event showed right-lateral strike-slip on an almost vertical fault, which is also
supported by structural observations from the field (Kastelic et al., 2008). The second event and its aftershocks also involved
115   oblique right-lateral reverse mechanisms. A number of smaller earthquakes with right-lateral mechanisms occurred in the
Slovenia-Croatia border area (Herak et al., 1995, 2009; Čarman et al., 2011; Jamšek Rupnik et al., 2016; Fig. 1). Vičič et al.

(2019) relocated microseismicity data covering 2006 - 2017. They discovered swarm activity related to the Raša, Predjama, Idrija, Ravne, and Selce faults down to 20 km depth on almost vertical fault planes.

Historical seismicity in western Slovenia includes several earthquakes exceeding magnitude 5.5 (Ribarič, 1982; AHEAD, 2020, Fig. 1). None of the reported events can be conclusively tied to a specific fault, and there is no apparent clustering on any of the known active structures. Reliable historical data is mainly confined to the last 200 years (e.g., Herak et al., 2009, 2017, 2018; Cecić, 2015). Modelling of the macroseismic effects of the M_w6.1 Ljubljana earthquake indicates that it occurred on one of the strike-slip faults that belong to the eastern part of Dinaric Fault System south of Ljubljana (Tiberi et al., 2018). The strongest historical event in western Slovenia was the 1511 Idrija earthquake (Ribarič, 1979; Fitzko et al., 2005; Cecić, 2011; Camassi, 2011). It devastated the mining town of Idrija in Slovenia and caused significant damage in NE Italy (see summary in Fitzko et al., 2005). Fitzko et al. (2005) modelled the macroseismic data and found the best fit for a 50 km-long rupture of the Idrija Fault, corresponding to a M6.9 dextral strike-slip earthquake. This is supported by geophysical studies and a paleoseismic trench in the village of Srednja Kanomlja near Idrija (Bavec et al., 2012, 2013). However, Falcucci et al. (2018) trenched the Colle Villano Thrust in NE Italy and found a post-15th century surface-rupturing earthquake, which they interpret as the 1511 event. Thus, it is still not resolved whether the 1511 Idrija Earthquake was a single event or if two earthquakes ruptured two different faults in close succession.

3 Methods

In order to identify the most promising sites for paleoseismological trenching, we first analysed the 1 m digital elevation model (DEM) of Slovenia (Ministry of the Environment and Spatial Planning, Slovenian Environment Agency, 2011). These data are freely available for the entire country and were collected using the LiDAR technology (Light detection and ranging; airborne laser scanning). We manually inspected the mapped traces of the Predjama and Idrija Faults and searched for offset geomorphic markers, breaks in slope, scarps, and similar indicators of recent tectonics. Then we identified sites with sediment archives that could have recorded large past earthquakes. For selected sites we acquired aerial images using a DJI Phantom 4 drone, which allowed us to compute high-resolution DEMs with up to 5 cm resolution using the structure-from-motion technique (SfM).

Geophysical surveys were then used to image the shallow subsurface and to precisely map the fault traces. All geophysical data are available online (Grützner et al., 2020). We used a ground-penetrating radar (GPR) system from Geophysical Survey Systems Inc (GSSI) with monostatic 100 MHz, 270 MHz, and 400 MHz antennas and a Pulse EKKO Pro Sensors & Software system equipped with bistatic 250 MHz antennas. All data were processed with the ReflexW software (Sandmeier Geophysical Research). Processing included frequency bandpass filtering, background removal, gain adjustments, and topographic corrections. The topographic data were extracted from the 1 m DEM.

Electric resistivity tomography (ERT) was performed with a 4-point-light system (Lippmann Geophysikalische Messgeräte). We used up to 80 electrodes with varying electrode spacing for Wenner, Schlumberger, and Dipole-Dipole arrays, depending

on target resolution and depth. Data inversion was done with Res2DInv (Geotomo Software) and included manual de-spiking
150 and topographic corrections.

Along several profiles we measured the vertical gradient of the geomagnetic field and the total magnetic field strength with a
proton magnetometer GSM - 19T (GEM Systems). The system consists of a rover and a base station, which allows correcting
the data for diurnal variation. We used 1 m point spacing along several long transects.

Based on the geophysics results we selected one trench site at the Predjama Fault and one at the Idrija Fault. The trenches were
155 excavated with a backhoe and their walls were cleaned and straightened. We installed a 1 x 1 m string grid, sketched the walls
in 1:10 scale, and produced 3D models and orthophotos of the trench walls using the SfM technique. Radiocarbon dating was
performed by BETA Analytic on charcoal and bulk organic carbon samples.

4 Results

4.1 Predjama Fault

160 #### 4.1.1 Structural Data

The Predjama Fault trench site is located on the Banjšice Plateau, northwest of the Čepovan Canyon. In this area, a single fault
trace is clearly visible in the DEM (Fig. 2). At Avče in the Soča Valley to the NW of our trench site, Moulin et al. (2016)
describe a prominent change in valley topography caused by the fault (Fig. 2). The fault bifurcates just SE of our trench site
and the two strands offset the cliffs of the Čepovan Canyon (Moulin et al., 2016). These authors also describe the prominent
165 vertical offset across the two fault strands. We found that slickensides in two quarry outcrops on each strand show almost pure
right-lateral strike-slip on fault planes dipping steeply to the SW (Fig. 3a-c). To the SE of the Čepovan Canyon, the two strands
of the Predjama Fault cross the Trnovski Gozd Plateau, but only the southern fault trace continues further to the southeast (Fig.
2). We chose our trench site partly based on these observations in order to capture the entire slip of the fault on a single trace
and to not miss significant portions due to its branching.

170 #### 4.1.2 Geomorphological observations

At the trench site we observed a prominent break in slope on a gently NE-dipping meadow (Fig. 3d-f). The break in slope is
detectable for ~200 m. To the NW and to the SE of our trench site, the scarp disappears in the steep and forested terrain.
Topographic profiles extracted from the 1 m LiDAR DEM and a 5 cm drone DEM reveal a systematic vertical offset of ~0.5
m on an uphill-facing scarp. In some, but not all places the scarp coincides with tracks used by the local farmers. Following
175 the argument of Copley et al. (2018) the break in slope is unlikely to be caused by a dirt road. In case the break in slope was
solely caused by a dirt road, the break in slope would be local only. However, we find a systematic offset of the entire slope.
Slovenian cadastre data from the early 19th century show no road, property boundary, or any other artificial feature at the
location of the scarp. The area was the scene of the 12th Battle of the Isonzo in 1917. Here, the Italian defence lines were

running ~N-S just before the attack of the Austria-Hungarian armies on 24 October (Glaise von Horstenau, 1932). The
180   Regional Archives Nova Gorica (Pokrajinski arhiv v Novi Gorici, https://www.pa-ng.si/) holds no aerial photographs from
World War I from our trenching area, but photos from nearby places on the Banjšice Plateau show intense modification of the
surface by military trenches and bomb craters. We carefully inspected the available high-resolution DEMs but did not find any
hints for military action or installations that left their traces in the morphology. However, Valjavec et al. (2018) found that
post-war landscape modifications have erased many traces of World War I in Slovenia. We also inspected the LiDAR data and
185   the drone DEMs for evidence of landsliding or soil creep but did not find any such feature. The straight trace of the scarp, the
systematic offset of the entire meadow, the lack of evidence for anthropogenic modification, and the fact that the scarp
coincides with the mapped fault trace led us to interpret it as the surface expression of the Predjama Fault and to focus our
geophysical prospection on this site.

4.1.3 Geophysics survey

190   We used GPR, ERT, and magnetic measurements on parallel profiles perpendicular to the scarp in order to check the subsurface
conditions and to select the most promising trench site (Fig. 4). Georadar did not provide good data quality, which during
trenching turned out to be due to highly conductive clayey sediments present near the surface. The geomagnetic data showed
neither hints for the fault nor for metal objects in the ground, which indicates the lack of potentially dangerous war remains.
The dipole-dipole ERT data with 1 m electrode spacing show mainly resistivities of less than 70 Ωm throughout all profiles
195   (Fig. 4). We interpret these low values as water-saturated, mainly clayey sediments. North of the break in slope we found a ~1
m thick layer with higher resistivities right below the surface in all profiles. Profiles 1 - 5 show values of 100-200 Ωm for this
layer; profiles 6-10 show values of up to 400 Ωm. These values likely correspond to a drier topsoil in the northern part of the
profiles. Due to the north-dipping slope and the high trees at the margin of the meadow, the southern part of the profiles is
shaded much longer than the northern part. This may explain the differences in soil humidity. In profile 4 - 10 we observe
200   another anomaly with increased resistivities at about 4 m depth just north of the break in slope. Based on the findings in the
trenches (Fig. 5, supplement 1-4), we interpret this anomaly as calcarenites and limestones that were brought closer to the
surface by the Predjama Fault. High resistivities were also encountered in profiles 6 - 9 at ~3 m depth and below in the
southernmost parts of the survey, which we assume to correspond to bedrock (also see trench logs in the next section).
Paleoseismic trenching took place after the geophysical survey and helped to better understand the resistivity pattern. However,
205   prior to trenching the significant variations in resistivity below the break in slope lead us to conclude that we found the trace
of the fault and that the site is suitable for further investigation. We chose the location of profiles 5 and 7 to open two trenches
(Figs. 4, 5; supplement 1-4).
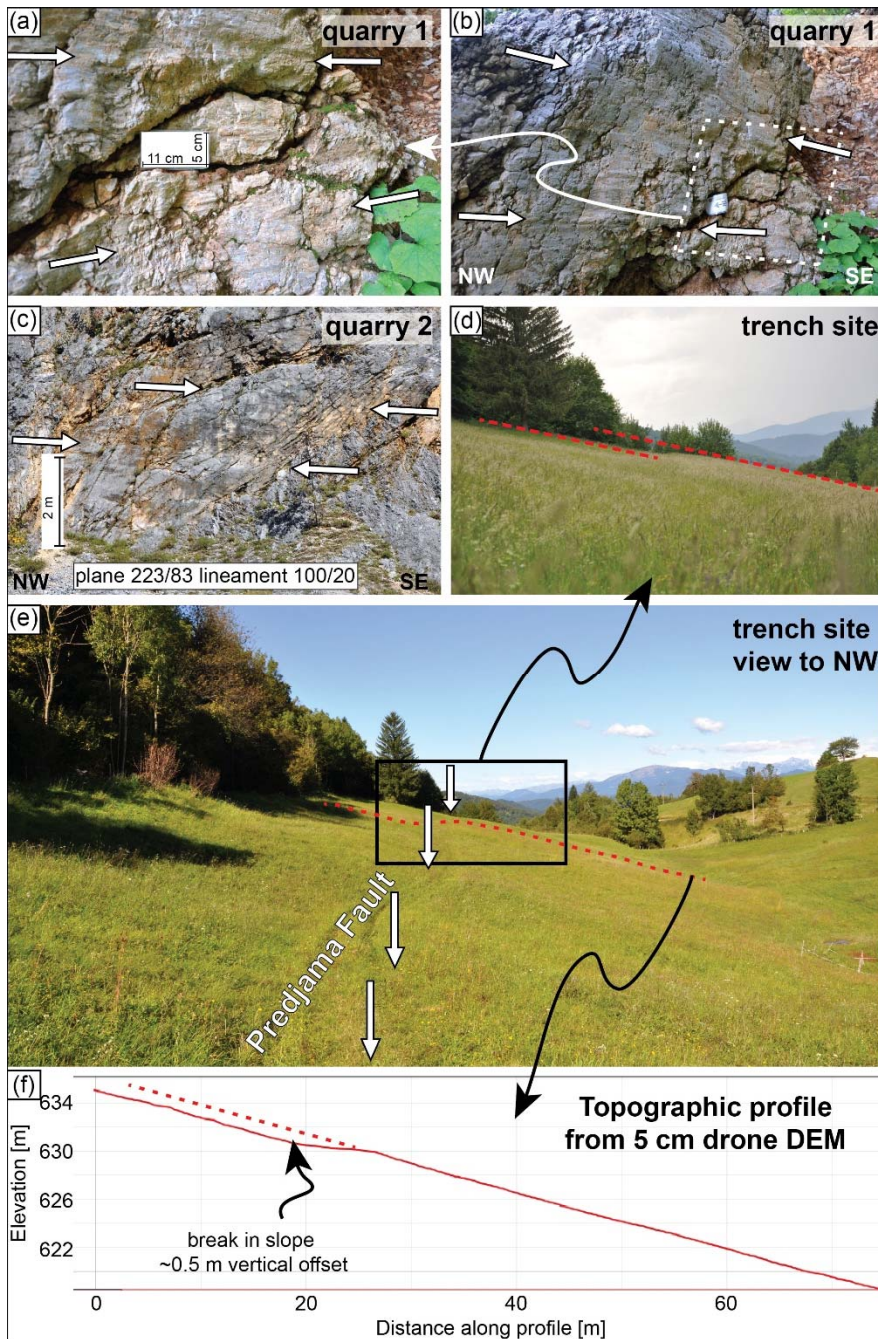
Figure 3: Investigation sites at the Predjama Fault. (a) At the southern strand of the fault, quarry 1 (N46.0299° E13.7632°) exhibits
E-W lineaments with right-lateral shear sense on a fault plane dipping steeply to the SW. (b) Larger section of the striated surface
in quarry 1. (c) Large SW-dipping fault planes are present at the northern fault strand in quarry 2 (N46.0506° E13.7485°).
Slickensides show almost horizontal right-lateral motion. (d) A break in slope offsets the trench site. The red dashed lines show
~0.5 m vertical offset. (e) NW view of the trench site (also see Fig. 4 for location). The red dashed line marks the location of the
topographic profile in (f). Trench 1 was opened across this profile. (f) Topographic profile from a drone DEM with 5 cm
resolution, illustrating the systematic offset of the slope and the uphill-facing scarp.
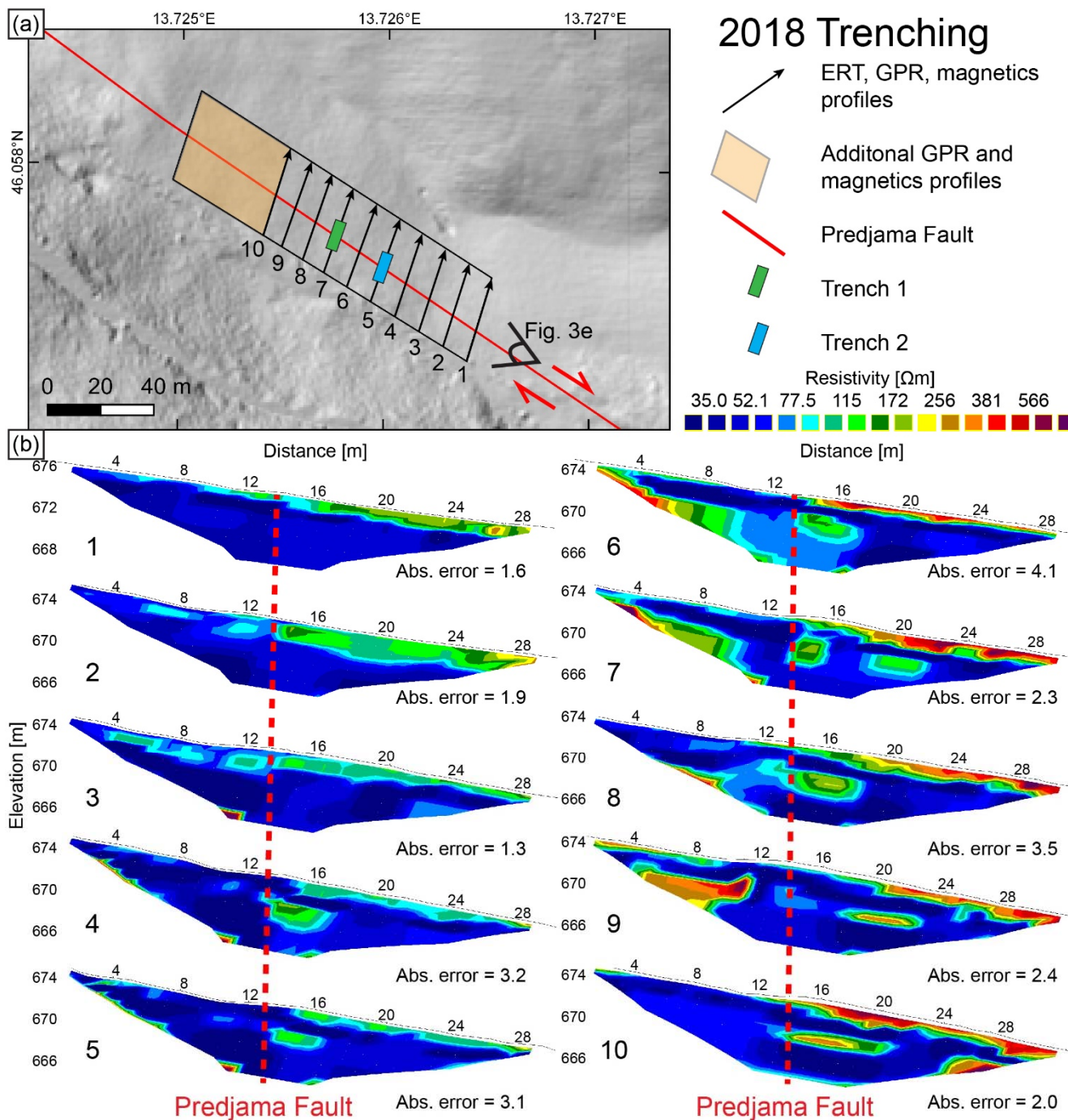
Figure 4: Map of the trench site at the Predjama Fault and ERT data (a). Black arrows mark the location of geophysical profiles (ERT, GPR, magnetics). Additional GPR and magnetics data were collected further to the NW. Seven iterations were used to invert the dipole-dipole ERT data (b). The ERT data show abrupt changes in resistivity below the break in slope, interpreted as the Predjama Fault trace (red dashed line).

220

4.1.4 Paleoseismic trenching

Trench 1 was 10 m long and on average 1.5 m deep (Fig. 5). Deeper excavation was prohibited by the shallow groundwater level. We distinguished seven units in both trench walls. Since both trench walls show comparable features, we use the north-western trench wall for the detailed description in the following. Unit U1 at the base of the trench consisted of clast supported,

225 intensely fractured and weathered calcarenites in a clayey matrix. Occasionally, larger and more coherent blocks of calcarenites were encountered in the upper parts of this unit (unit U2). Both units show a dip towards the NE. On top of U1 and U2 sits a thin layer of massive grey clay, unit U3. It is overlain by a thin red ribbon of sandy clay (unit U4), that mainly consists of weathered calcarenites. Both U3 and U4 dip to the NE. Most of the upper part of the trench is made up of massive brown clays (unit U5). The contact between U4 and U5 is sharp. Where U5 is in contact with U4, it contains small amounts of sand and

230 fine gravels as well as charcoals. Thus, U5 is not just the product of weathered bedrock, but also involves slope deposits. The pale, bleached clay unit U6 with up to 30 cm thickness occurs just beneath the recent soil (unit U7). We note that unit U6 is not necessarily a sedimentary body, but the distinct pale appearance may be due to post-depositional modification by increased water content, or it may result from compaction due to the occasional use of the track by the farmers. No sharp fault trace was found in the trench. Instead, we observe a zone of localised deformation at around 4-5 m distance from the southern end of the

235 trench.

Unit U1 can be easily identified in the first five metres of the trench. Around 5 m distance from the southern end of the trench, this unit appears to bend down together with the overlying units U3 and U4. In a 40 cm-wide gap unit U5 reaches the bottom of the trench. Unit U1 then occurs again between 5 - 6 m and between 6- 8 m with up to 0.6 m thickness. It becomes gradually more weathered upwards and the contact with unit U5 is not sharp. The larger blocks of intact calcarenites that make up unit

240 U2 are present throughout the trench and show no deformation.

Unit U3 is only visible in the southern section of the trench for about 2 m. It has a more constant thickness of 10 cm in the SE wall of the trench and varies between 10 cm and 20 cm thickness in the NW trench wall. While this unit parallels the top of unit U1 for about 2 m from its southern end, it then bends down and dips steeply towards the NE beneath the break in slope. Here we observe small folds in the tip of the layer.

245 A similar feature is observed in unit U4, which also parallels U1, but then bends down into a steeply dipping fold. Here we identified small horizontal faults with <5 cm offset cutting the layer. The tip of the unit flattens again to almost the same dip angle as its southern part, with a vertical offset of 30 cm. The few coarser grains at the contact between U4 and U5 show that also the lowermost part of U5 bends down parallel to U4. The bending, the folding, and the faulting observed in this layer coupled with geomorphological and geophysical observations led us to interpret the deformation as tectonically induced. A

250 sample of organic material from the contact between U4 and U5, sample SLO19_BAN3, gave an age of 8406-8311 cal BP (Table 1). Note that we sampled a fragment of charcoal, but during sample preparation in the lab it turned out to be too small, but it was possible to date the organic sediment around it.
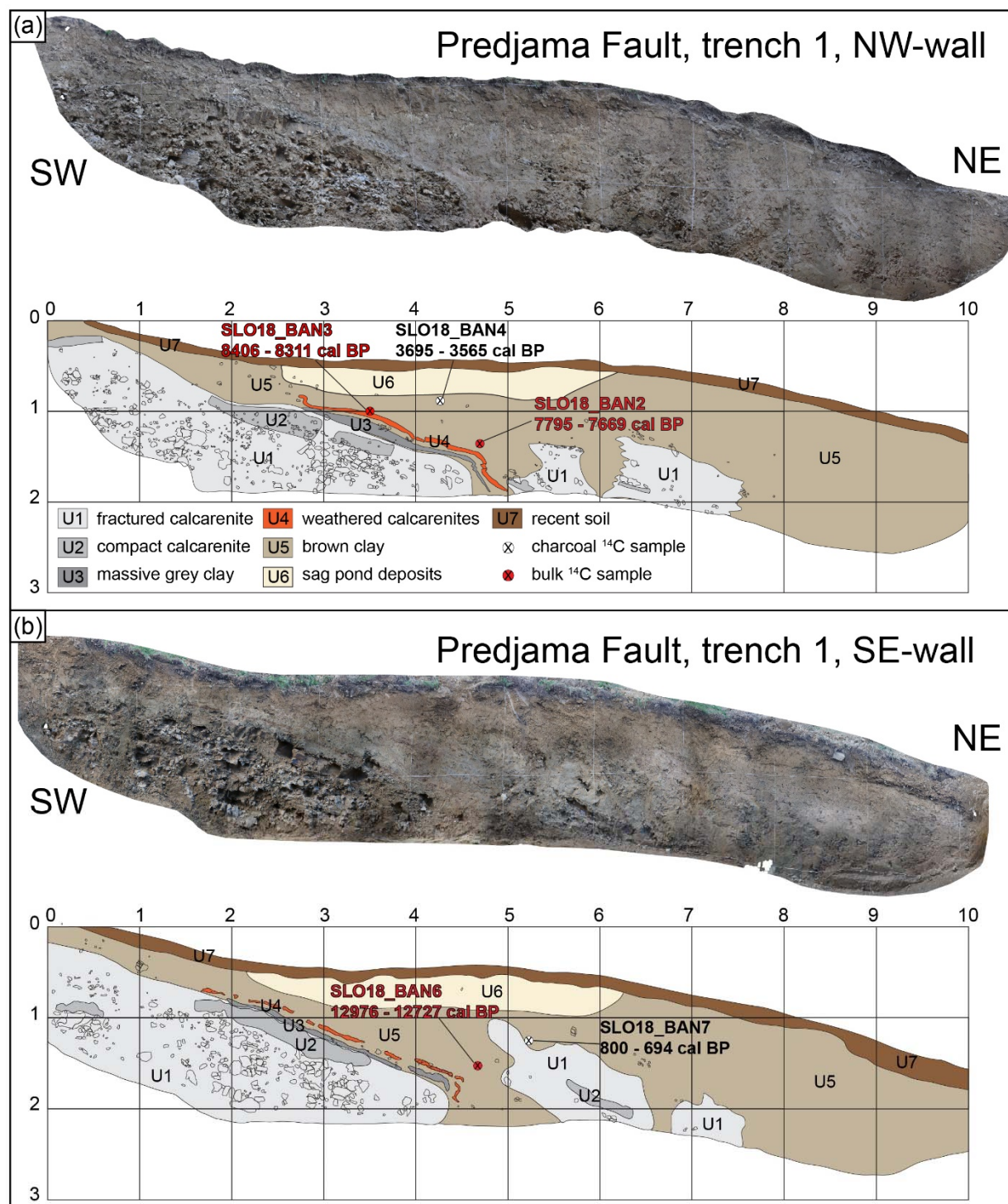
Figure 5: Paleoseismic trench 1 across the Predjama Fault on the Banjšice Plateau. (a) NW-wall of the trench. The fault crosses the trench at ~5 m distance. Note the folded units U3 and U4. (b) SE-wall of the trench. The fault crosses the trench between 4 m and 5 m distance.

255

Unit U5 shows no hints for tectonic deformation except at the contact with U4, but the massive plastic clays may simply obscure any hints for faulting or folding. We dated a bulk sediment sample (SLO19_BAN2) from 10 cm above U4. This sample gave an age of 7795-7669 cal BP. A charcoal sample (SLO19_BAN4) from right below U6 provided an age of 3695-
260   3565 cal BP. All these ages are in stratigraphic order. On the opposite trench wall, we also dated U5 with a bulk sample (SLO19_BAN6) that returned an age of 12976-12727 cal BP and a stratigraphically higher charcoal sample (SLO19_BAN7) that showed an age of 800-694 cal BP. These two samples are significantly older and younger than those of U5 on the NW trench wall, respectively.

Unit U6 can only be observed for around 4 m on either trench wall. Its pale colour and the position right below the break in
265   slope and above the zone of folding lead us to interpret it as a sag pond post-dating tectonic deformation. Alternatively, it could be compacted soil resulting from the occasional use of the break in slope as a dirt road. Its age is constrained by samples SLO19_BAN4 and SLO19_BAN7 to post-800 BP. The full high-resolution trench orthophotos are presented in the supplement.

Trench 2 exhibited a different stratigraphy. Here, we observed massive brown and grey clays beneath the modern soil, but no
270   calcarenites. Instead, the base of the trench at ~2 m depth was made up in its southern part by limestone clasts in a brown clayey matrix. Attempts to excavate deeper than 2 m were prohibited by the groundwater level. A possible fault zone in the centre of the trench is marked by a colour change in the clays and the termination of the limestone clast layer. However, the uniform clays and the lack of clearly deformed markers led us to not speculate about evidence for faulting in the trench. A high-resolution orthophoto of both trench walls is provided in the supplement.

275

4.2 Idrija Fault

The Idrija Fault trench site is located 4.5 km NW of the town of Idrija, in the valley of the Kanomljica River (Fig. 2). Cunningham et al. (2006) noted that several drainage anomalies around the Kapa hill just to the SW of our trench site point to Late Quaternary or even Holocene fault motion (Fig. 6). Bavec et al. (2012, 2013) chose the river valley at the SW foot of the
280   Kapa hill for a geophysics study and for a paleoseismological trench. Moulin et al. (2014) analysed the geomorphology in detail and reported between 340 m and 380 m of right-lateral offset based on the correlation of the modern Kanomljica river and abandoned valleys. The precise trace of the Idrija Fault in the vicinity of our trench site is subject to some debate (Fig. 6; also see Moulin et al., 2014). The NW flank of the Kapa hill exhibits a wide shear zone with (ultra-)cataclastic rocks. This wide shear zone is in line with the observation that the Idrija Fault has a large cumulative offset (Čar, 2010; Placer et al., 2010).
285   The trace of the fault in the wide valley of the Kanomljica is obscured by flat-lying fluvial sediment. Outcrops on the north side of the valley show that at least one fault strand clearly runs along the base of the hills (Moulin et al., 2014).
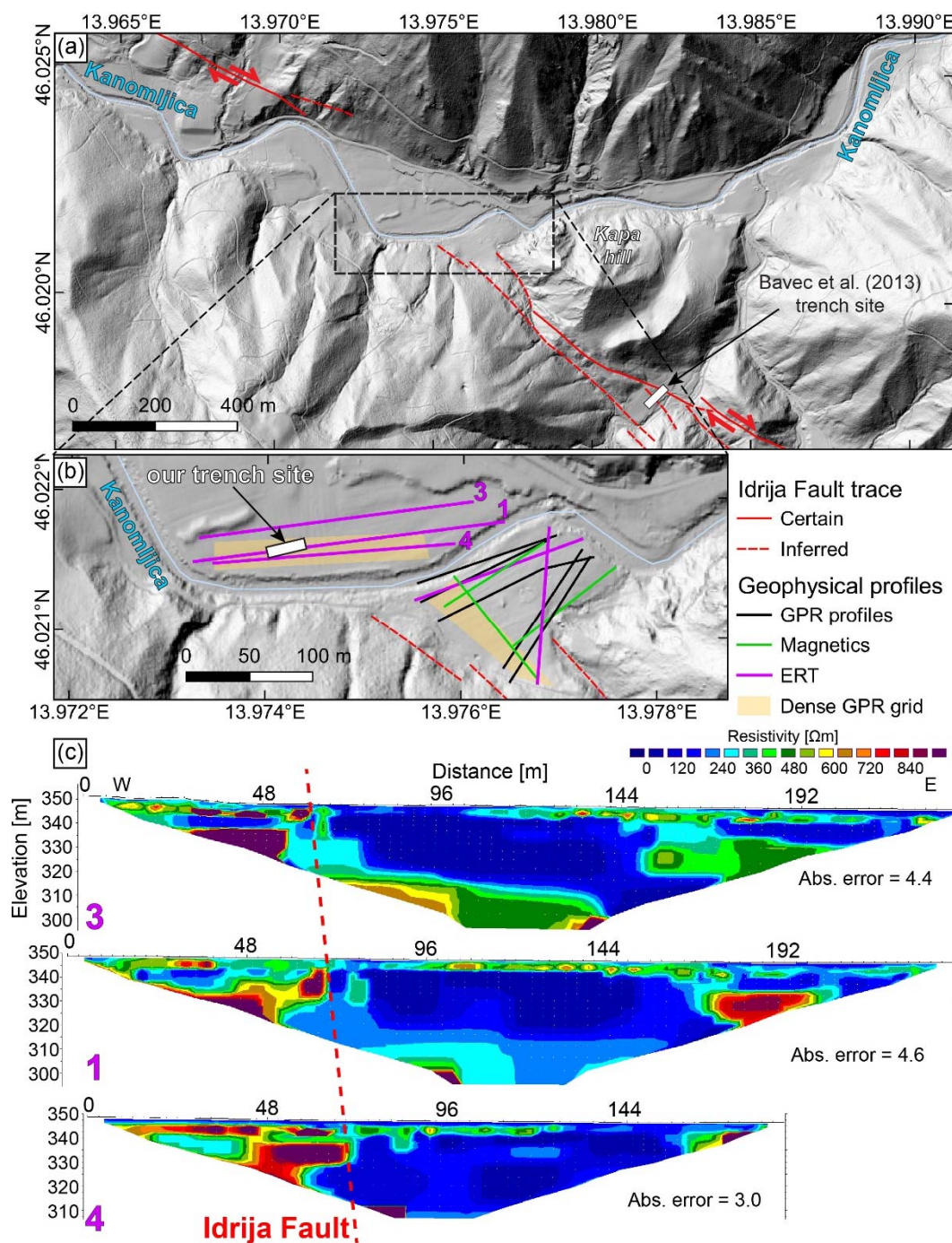
Figure 6: Map of the trench site at the Idrija Fault and selected ERT data. (a) Setting of the trench site and mapped traces of the Idrija Fault after Cunningham et al. (2006), Bavec et al. (2013), and Moulin et al. (2014). The precise fault trace is unknown in the flood plain of the Kanomljica River. (b) Detailed view of the location of all geophysical profiles used for trench site selection. (c) ERT profiles 1, 3, and 4 that were crucial for trench site location. Red dashed line indicates the interpreted fault trace. All data show dipole-dipole configuration with ten iterations in the inversion.

290

4.2.1 Geophysics survey

295 We concentrated our geophysical investigations on the flat area of the Kanomljica valley because we expected to find deformed sediments in case the fault ruptured the surface in the Late Quaternary (Fig. 6). Additional surveys were performed on the southern bank of the Kanomljica. The geomagnetics survey was not successful. Not only did the data quality suffer from the presence of power lines and other anthropogenic disturbances, but also in areas not affected by these effects we could not identify a signal pointing to a change in the subsurface structure. Georadar data suffered partly from low penetration depths

300 owing to clay-rich sediments and a low groundwater table. Although some information on the geometry of the fluvial units could be extracted, we did not see any clear evidence for faulting that would have allowed for picking a promising trench site. The ERT profiles on the flat surface north of the Kanomljica showed the clearest hints for the location of the Idrija Fault. For these profiles we used 3 m electrode spacing in order to reach great depths (Fig. 6). The uppermost part of the subsurface is made up of a medium-resistivity layer (200-700 Ωm) of about 3-5 m thickness, which likely corresponds to the sediment fill

305 of the valley. In the trenches that we opened after the geophysics campaign we found that the sediments are dominantly coarse fluvial gravels, and that the groundwater table is below 2 m depth. This explains the observed range of resistivities.

Below the medium-resistivity layer, the central parts of the profiles are characterised by an up to 30 m thick low-resistivity unit (<200 Ωm). The western parts of the profiles, however, show high resistivity units of more than 700 Ωm. The contact between the two is sharp and mostly vertical. In profiles 1 and 4, the contact is at 69 m profile distance. In profile 3, the contact

310 is at 60 m. We interpret the low resistivity unit as the crushed bedrock of the wide fault zone and the high-resistivities as the intact, non-faulted bedrock. This is supported by our field observations of cataclastic rocks along the mapped and inferred fault trace. Furthermore, Bavec et al. (2012) found the same pattern in their geoelectric profiles SE of Kappa Hill. Their trench (Bavec et al., 2013) confirmed the low resistivity of the faulted bedrock. These authors also found the active fault strand at the contact between the units of high and low resistivities. Consequently, we interpret the contact between the high-and low-

315 resistivity units as the location of the fault. This contact lies in the projection of the inferred SW fault strand of Bavec et al. (2012). In the eastern parts of the three profiles presented in Fig. 6, sharp contacts between the low resistivity units in the centre and medium to high resistivities (300-800 Ωm) further east can be seen. These zones are located at 170 m, 150 m, and 160 m distance in profile 1, 3, and 4, respectively. The contacts do not align as well as the ones in the western part of our survey area, and they are located approximately in the projection of the NE fault trace (Fig. 6; Bavec et al., 2012). A power

320 line was present above these parts of the profiles, which may have distorted the measurements here. However, we interpret this pattern as the NE edge of the inner fault zone following the reasoning above.

4.2.2 Paleoseismic trenching

Based on the ERT data we decided to open a trench across the sharp contact between the high resistivity units and the low resistivity units in the western part of the survey area (Fig. 6). The trench was 20 m long, 2 m deep, 2 m wide, and placed on

325   the track of profile 1. We did not dig any deeper because the nearby Kanomljica stream incised about 2 m into the flat valley bottom, and the groundwater table was located just beneath the trench floor. In the following we only describe the central part of the trench where we encountered traces of recent deformation. The full high-resolution trench orthophotos are presented in the supplement.

     In general, the trench is characterised by fine to coarse gravel deposits. In the centre of the trench, a channel exhibits clayey to
330   sandy units. In the north wall, the channel can be seen between 5.5 m and 12.5 m distance, reaching down to the trench floor (Fig. 7a). In the southern trench wall, the channel is observed between 4 m and 14 m distance in up to 1 m depth (Fig. 7b). We observed eleven different units in the trench. Unit U1 consists of clast-supported, fine-coarse fluvial gravels in a brown clayey matrix. This unit is present throughout the entire trench. Unit U2 is made up of mostly medium gravels in a bright red, clayey matrix. This layer is situated within unit U1 and only visible in the northern wall. Fine to coarse gravels in a light red
335   clay matrix (unit U3) can be found as pockets in both trench walls within U1. At the base of the channel, we identified U4, consisting of sandy silt with yellow flakes. This unit is in vertical contact with massive grey clays (unit U5) and overlain by yellowish clayey gravels (unit U6). In the southern trench wall, U4 partly overlies U5, which may indicate that it has eroded into the latter. Only in the northern trench wall, a small pocket of grey clayey sands (unit U7) is present at the contact between U1 and U8/U10. In the southern trench wall, silty-sandy, dark grey unit U9 cuts through units U5 and U8. Both units U4 and
340   U6 terminate at U9. Unit U9 is overlain by the darkest parts of U10, to which there is no sharp boundary.

     Unit U10 consist of gravels in a matrix of grey clays. This unit overlies U7 in the northern trench wall and units U5 and U6 in the southern trench wall. The upper part of the channels is made up by massive grey and brown clays of unit U10. We found white speckles at the base of U10 between 7 m and 9 m distance (N wall) and between 11 m and 12 m distance in the southern trench wall. Unit U10 is overlain by the recent soil (unit U11).

345   We interpret most of the units in the northern trench as undisturbed fluvial sediments. Between 8 m and 9 m distance, however, we observe several features that point to tectonically induced deformation. Units U4 and U6 show vertical terminations at their eastern ends, where they are in contact with U5. A charcoal sample dates U5 to 2140 - 1987 cal BP. The base of U5 fills the space between larger blocks (Fig. 7c). It remains unclear whether this resembles a fissure fill, because of the lack of horizontally layered, fine-grained material here. Two bulk sediment samples from these lowest parts of U5 returned radiocarbon ages of
350   2645 - 2489 cal BP and 1528 - 1376 cal BP, respectively. Next to the base of U5 we encountered vertically aligned pebbles (Fig. 7c). This is the only occasion of aligned pebbles in the entire trench. Right above these pebbles sits a large (~40 cm diameter) clast that is intensely fractured, but not offset. The cracks have no preferred orientation, and their surfaces show slightly different colours than those of fresh hand specimens that we hammered off the clast. The fractures were clearly not caused by the excavator. This is the only fractured clast that we have found in the trench. U5 is in the northern wall overlain
355   by U10, which was dated to 2307 - 2056 cal BP and 492 - 315 cal BP by two charcoal fragments. Unit U8 resembles a pocket of coarse material emplaced into the clays of U10. We did not encounter any faults that bound U8, but we note its suspicious position above the aligned pebbles and the fractured clast.
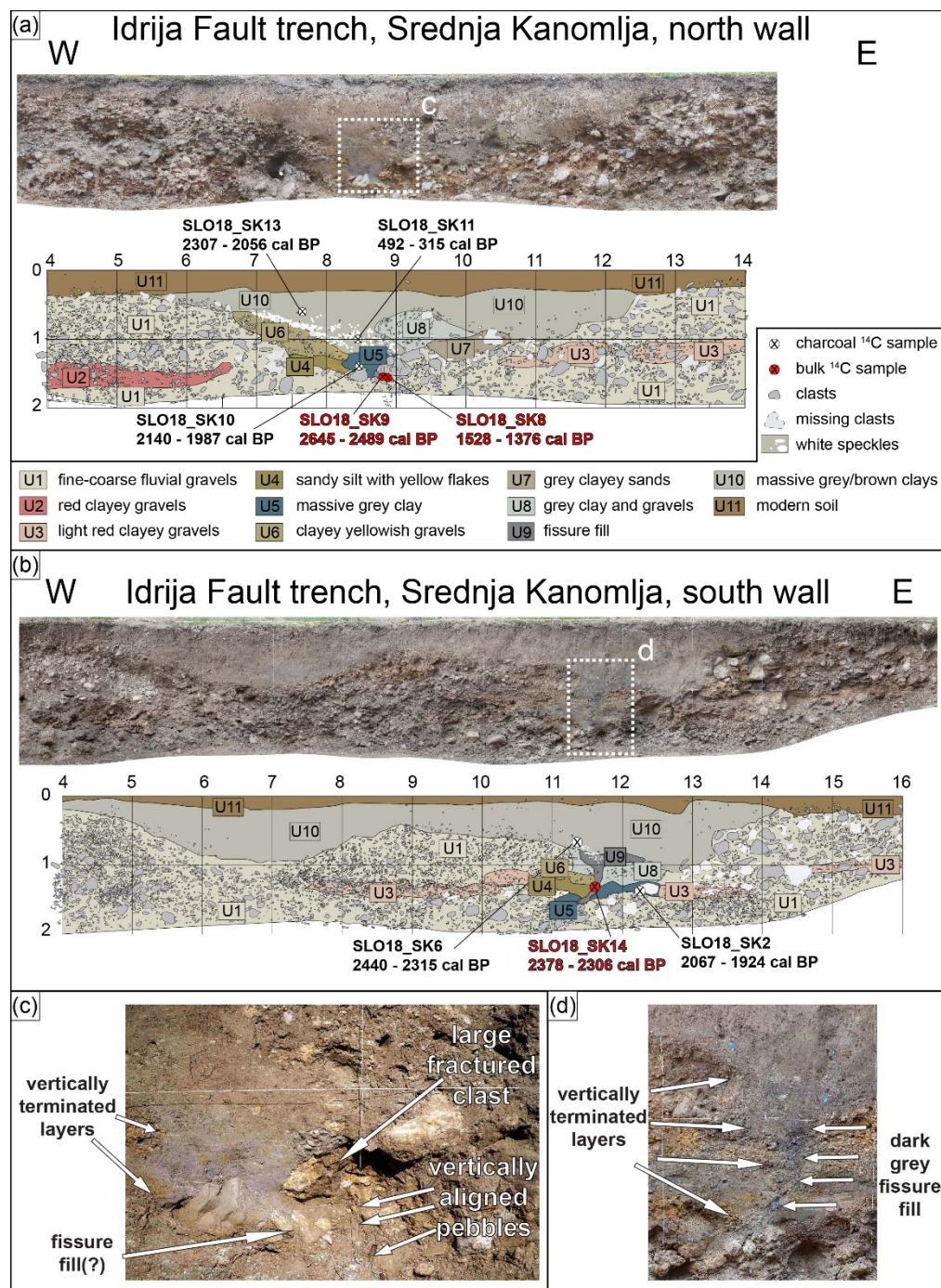
Figure 7: Results from the Idrija Fault trench at Srednja Kanomlja. (a) Orthophoto and trench log of the northern trench wall. (b) Orthophoto and trench log of the southern trench wall. Note that the photo and log have been flipped for easier comparison with the northern wall. (c) Close-up photo of the fault zone in the northern trench wall. Note the vertically terminated layers and the aligned pebbles below the massive, fractured clast. (d) Close-up photo of the fault zone and the fissure fill observed in the southern trench wall.

360

In the southern trench wall, only a narrow zone shows evidence for tectonic deformation between 11 and 12 m distance. Similar
365 to the north wall, we observe vertical terminations of units U4 and U6. The most striking feature is the organic-rich, dark grey
U9. This unit is funnel-shaped and extends from the base of U10 about 1 m downwards. It is in vertical contact with U4 and
U6, and it cuts through U5 and U8 (Fig. 7d). We interpret U9 as a fissure fill, with the filling material sourced from the base
of U10. We excavated the fissure further into the trench wall to check if it may be due to a large root, but we found that the
feature is elongated and not round as it would be typical for roots. A bulk sediment sample from the fissure fill returned a
370 radiocarbon age of 2378 - 2306 cal BP. A charcoal fragment from U5 was dated to 2067 - 1924 cal BP. At the base of U10 we
collected a charcoal that gave an age of 2440 - 2315 cal BP.

Table 1: Summary of all dated samples. Probability was calculated after Bronk Ramsey (2009). Calibration was done with INTCAL13 (Reimer et al., 2013).

Sample ID	Fault	Trench	Material	d13C	Conventional age	Calibrated age (Probability)
SLO18_SK2	Idrija	S wall	Charcoal	-25.3 o/oo	2040 +/- 30 BP	2067 - 1924 cal BP (88.1%) 2111 - 2080 cal BP (6.8%) 1907 - 1904 cal BP (0.5%)
SLO18_SK6	Idrija	S wall	Charcoal	-	2340 +/- 30 BP	2440 - 2315 cal BP (94.5%) 2456 - 2449 cal BP (0.9%)
SLO18_SK8	Idrija	N wall	Organic sediment	-	1550 +/- 30 BP	1528 - 1376 cal BP (95.4%)
SLO18_SK9	Idrija	N wall	Organic sediment	-27.4 o/oo	2510 +/- 30 BP	2645 - 2489 cal BP (67.7%) 2740 - 2650 cal BP (27.7%)
SLO18_SK10	Idrija	N wall	Charcoal	-25.4 o/oo	2080 +/- 30 BP	2140 - 1987 cal BP (94.5%) 1958 - 1952 cal BP (0.9 %)
SLO18_SK11	Idrija	N wall	Charcoal	-24.9 o/oo	350 +/- 30 BP	412 - 315 cal BP (54.2%) 492 - 420 cal BP (41.2%)
SLO18_SK13	Idrija	N wall	Charcoal	-24.5 o/oo	2160 +/- 30 BP	2208 - 2056 cal BP (55.4%) 2307 - 2228 cal BP (40%)
SLO18_SK14	Idrija	S wall	Organic sediment	-28.3 o/oo	2320 +/- 30 BP	2378 - 2306 cal BP (89.9%) 2235 - 2184 cal BP (5.5%)
SLO18_BAN2	Predjama	T1, NW wall	Organic Sediment	-24.0 o/oo	6900 +/- 30 BP	7795 - 7669 cal BP (95.4%)
SLO18_BAN3	Predjama	T1, NW wall	Organic sediment	-	7530 +/- 30 BP	8406 - 8311 cal BP (93.9%) 8235 - 8221 cal BP (1.5%)

SLO18_BAN4	Predjama	T1, NW wall	Charcoal	-23.2 o/oo	3380 +/- 30 BP	3695 - 3565 cal BP (95.4%)
SLO18_BAN6	Predjama	T1, SE wall	Organic Sediment	-23.8 o/oo	10980 +/- 40 BP	12976 - 12727 cal BP (95.4%)
SLO18_BAN7	Predjama	T1, SE wall	Charcoal	-24.5 o/oo	860 +/- 30 BP	800 - 694 cal BP (83.5%) 901 - 866 cal BP (9.9%) 826 - 814 cal BP (2%)

5 Discussion

5.1 Earthquakes on the Predjama Fault

The combination of geomorphological data, geophysical prospection, and paleoseismological trenching reveals that the Predjama Fault has been active in the Holocene. Two main observations allow deducing a recent surface-rupturing seismic event: (i) the uphill-facing scarp and (ii) the folded and faulted layers in the trench. The detectable break in slope is rather short (~200 m), but it perfectly matches the mapped fault trace, it is located right above the geophysical evidence of faulting, and an anthropogenic origin is as unlikely as a mass movement (cf. Copley et al., 2018). The bend in the trace of the Predjama Fault at our trench site (Fig. 2, inset) leads to a local transpressive regime, which allows for significant vertical offsets. Moulin et al. (2016) also describe the long-term vertical offset along the Predjama Fault between our trench site and the Čepovan Canyon. However, our structural data, long-term offsets at the edge of the Čepovan Canyon (Moulin et al., 2016), and vertically aligned microseismicity below the fault trace (Vičič et al., 2019) show that the fault is predominantly, albeit not purely, strike-slip.

In addition to the morphological evidence, the trench (Fig. 5) exhibits fault-perpendicular shortening. In the northern trench wall, we observe a vertical step of ~0.4 m in unit U1 between 4 m and 5.5 m distance (north side up, same as the scarp). In the southern trench wall, this step is harder to measure because unit U1 does not have a sharp boundary. The offset of unit U2 is the better marker here and indicates ~0.6 m of vertical offset between 4 m and 6 m distance. These observations fit very well with the presence of the sag pond deposits (U6) on top of the deformation zone, which we interpret to have formed after the last uplift event. U6 is only compacted soil due to the occasional use of the break in slope as a dirt road, it is likely that the local farmers took advantage of this morphological scarp. The offsets also fit with the height of the scarp. Both trench walls show folding, minor-scale faulting, and a downward bend of the prominent reddish marker horizon, unit U4. The observed deformation cannot be explained with soil creep, mass movements, or anthropogenic modification. Although we cannot pin down the exact fault trace, the sharp breaks in unit U4 and the sag pond deposits point to rapid shortening. We therefore conclude that the deformation has been caused by at least one surface-rupturing earthquake. The lack of clearly identifiable, thin sedimentary layers makes it impossible to decide whether only one event or several earthquakes were recorded in the trench.

5.2 Dating of the Predjama Fault earthquake(s)

400 In the northern trench wall, all three radiocarbon samples are in stratigraphic order. The stratigraphically lowest sample from U4, sample SLO18_BAN3, was submitted as a charcoal, but in the lab it turned out that the sample size was very small and that only the surrounding organic sediment could be treated. This sample, however, gave an age of 8406 - 8311 ka cal BP (table 1). Bulk sample SLO18_BAN2 is located just a few centimetres above U4 and returned a slightly younger age of 7795 - 7669 cal BP. Taken together, these two samples indicate that the deformation happened after ~8.4 ka, because U4 is deformed.

405 Charcoal sample SLO18Ban_4 has an age of 3695 - 3565 cal BP and immediately pre-dates the formation of the sag pond U6. In the southern trench wall, a bulk sample from unit U5 close to the deformation zone gave an age of 12976 - 12727 cal BP (SLO18_BAN6). The stratigraphically higher sample SLO18_BAN7 (charcoal) is much younger with an age of 800 - 694 cal BP. While samples SLO18_BAN2 and SLO18_BAN3 are consistent, sample SLO18_BAN6 is much older than those two but should give a similar age. This can either be explained by the inherent large uncertainties related to the dating of bulk samples

410 (e.g., Wang et al., 1996; Howarth et al., 2018; Langridge et al., 2020), or by the (unknown) lateral component of fault motion that juxtaposes units of different age. Likewise, the two charcoal samples SLO18_BAN4 and SLO18_BAN7 are 3 ka apart, although they were expected to give similar ages. One explanation is that the older sample has a residence time issue, that is, the charcoal could stem from an old tree and it could have rested somewhere upslope before deposition in the present-day location (see discussion in Zachariasen et al., 2006). Another explanation is again the unknown lateral component of fault

415 motion. The most conservative approach for bracketing the age of the observed deformation is to use the oldest and the youngest samples, which would place the earthquake(s) between 13 - 0.7 ka. However, the good agreement of the samples in the northern trench wall leads us to speculate that the deformation actually happened after 8.4 ka. The young age of sample SLO18_BAN7 could explain why the scarp is still preserved.

5.2 Earthquake magnitude on the Predjama Fault

420 The fact that the scarp is relatively short may hint to a localised surface rupture, but it is more likely that the scarp is eroded or anthropogenically overprinted to the NW and to the SE of our trench site. Recent examples have shown that even earthquakes with magnitudes below M5.5 can cause surface ruptures, for example, the 2019 M_W4.9 Le Teil earthquake (Ritz et al., 2020) or the 2010 M_W5.0 Ecuador event (Champenois et al., 2017). Usually, these have small offsets and surface rupture lengths of a few hundred metres to several kilometres. The scarp at the Predjama Fault has a vertical offset of 0.5 m and a length of 200

425 m only, which is much higher than the slip-rupture length ratios reported from the literature (e.g., Wells and Coppersmith, 1994). There are rare cases, however, in which unusually short but high scarps have been observed (e.g, the 1992 M_S7.3 Suusamyr earthquake; Ghose et al., 1997). We rather use the offset than the length of the scarp for estimating paleo-earthquake magnitude.

The Predjama Fault is dominantly strike-slip (Fig. 3), but the lack of suitable markers hampers measuring the horizontal offset.

430 Therefore, the observed 0.5 m of offset must be taken as a minimum value. The empirical relationship of Wells and

Cop mith (1994) for the maximum displacement on all types of faults results in a magnitude of about $M_W6.4$ for 0.5 m offset. Using the self-consistent relationships of Leonard (2010) for strike-slip faults result in $M_W6.3$. Wells and Coppersmith's (1994) empirical relationship between fault length and magnitude would allow for a $M_W7.3$ earthquake if the entire 75 km-long Predjama Fault ruptured in one event. Using the Leonard (2010) for strike-slip faults, we also get $M_W7.3$. Such a large

435   earthquake would imply several metres of slip, for which we do not find geological evidence in our trench. We conservatively infer that the observed deformation features were caused by an earthquake of at least magnitude $M_W6.3$ if they were caused by one single event. Further support for this interpretation comes from the fact that no reports of surface ruptures are known for any of the strong historical earthquakes of up to M6.1 on the strike-slip fault system in W Slovenia (cf., Živčić et al., 2000). Only the M~6.8 Idrija earthquake has probably ruptured the surface (Bavec et al., 2013; Falcucci et al., 2018). Thus, the

440   earthquake that caused the offsets in the trench was likely much stronger than $M_W6.1$.

5.3 Earthquakes on the Idrija Fault

Our ERT data show that the strong vertical resistivity contrasts are situated along strike of the mapped Idrija Fault trace, and we found deformation structures at this very location in the paleoseismological trench. This leads us to conclude that we rightly identified the recently active fault trace. Four main observations from the trench are evidence for earthquake faulting in the

445   Holocene: (i) the filled fissure, (ii) the vertical terminations of fluvial sediments, (iii) vertically aligned pebbles, and (iv) a large, fractured clast. These four features were all found in a narrow zone that aligns with the mapped fault trace.

The fissure in the southern trench wall cuts through units U5 and U8. Units U4 and U6 terminate at the fissure. This geometry cannot be explained by sedimentary processes. The termination of layers in the southern trench wall probably results from lateral shifts of sedimentary bodies due to strike-slip motion on the fault. The fill consists of dark organic material that is also

450   present above the fissure. Therefore, we interpret that an open crack formed due to faulting in a strong earthquake, and that the material present at the surface fell in and filled the crack relatively quickly. We consider it unlikely that the fissure was caused by lateral spread or a failure of the riverbanks, perhaps due to seismic shaking, because the fissure is only localised and lacks a sliding horizon at its base. Also, no hints for liquefaction re observed. Recent examples of lateral spread show extensive cracks with large offsets that occur due to the shaking and often also in combination with liquefaction (e.g.,

455   Papathanassiou and Pavlides, 2007; Hayes et al., 2010; Cubrinovski et al., 2012). Instead, the fissure that we observe could resemble en echelon ruptures in a strike-slip earthquake, as it was frequently observed in recent events (c.f., Sylvester, 1988; Treiman et al., 2002; Talebian et al., 2004; Duman et al., 2005; Audemard, 2006; Barrell et al., 2011, Choi et al., 2018). This would explain why we did not observe a similar feature in the northern trench wall.

In the northern trench wall, we not only observed the vertically terminated layers, but also aligned pebbles and a large, fractured

460   clast. Aligned pebbles are described from many faults cutting through sediments world-wide (e.g., Hooyer and Iverson, 2000; Vanneste and Verbeeck, 2001; Sapkota et al., 2013; Patyniak et al., 2017; Zabcı et al., 2017). However, they are sometimes also related to liquefaction (e.g., McNeill et al., 2005), for which we do not find evidence. Although we found aligned pebbles only in one place in our trench, their location fits perfectly with the other indicators of active faulting. Right above these

aligned pebbles we found the only ruptured clast of the trench. Such ruptured clasts in a fault zone surrounded by intact clasts
465   have been described from faults around the world (e.g., Atwater, 1992; Radjai et al., 1998; Alfaro et al., 2001; Thakur and
Pandey, 2004; Silva et al., 2009; Agosta et al., 2012; Tokarski and Strzelecki, 2020; Tokarski et al., 2020). If the broken clast
were due to gelifraction, we would expect to find many fractured rocks and not only one right in the fault zone (cf., Bertran et
al., 2020). The fact that only one clast broke indicates that the fractures were not caused by the regional stress regime (cf.,
Ramsay, 1964; Eidelmann and Reches, 1992). Similarly, it is unlikely that the river transported only one clast with cemented
470   voids that later dissolved at the trench site. We conclude that all the observations described above prove a tectonic origin of
the observed features.

5.4 Dating of the Idrija Fault earthquake

In the northern trench wall, we obtained two radiocarbon ages from bulk organic material below the fractured clast (Fig. 7).
Sample SLO18_SK8 gave an age of 1528 - 1376 cal BP, sample SLO18_SK9 returned an age of 2645 - 2489 cal BP. These
475   two ages differ by at least 1 ka, which we attribute to the inherent uncertainties of dating bulk material. Charcoal sample
SLO18_SK10 from unit U5 dates to 2140 - 1987 ka BP. This is slightly younger than SLO18_SK9, which is in line with its
stratigraphic position. Thus, sample SKO18_SK8 likely underestimates the age of the unit below the fractured clast. A charcoal
sample from U10 right above U5, SLO18_SK11, is about 1.6 ka younger (492 - 345 cal BP) than U5, which is again in
stratigraphic order. However, another sample from unit U10 gives an older age of 2307 - 2056 cal BP (sample SLO18_SK13).
480   This rather old age can be explained by considering that unit U10 consists of washed-in material, which could include older
charcoal fragments with a complex history. The age of the younger charcoal (SLO18_SK11) gives a tighter constraint on the
deposition age of the unit (not older than 492 cal BP). From the northern trench wall, we can conservatively deduce that the
deformation occurred after the deposition of units U1-U6 (youngest unit dated is U5) and before the deposition of U10, hence,
between 2140 - 315 cal BP.

485   We obtained three samples from the southern trench wall. Sample SLO18_SK2 is from a charcoal from unit U5 and returned
an age of 2067 - 1924 cal BP. This fits perfectly well with the age of U5 in the northern trench wall and confirms that the age
of U5 is a proper upper boundary of the deformation seen in the trench. Unfortunately, only bulk organic material could be
sampled from the fissure fill. Sample SLO18_SK14 gave an age of 2378 - 2306 cal BP. This is older than unit U5, which was
cut by the fissure. We attribute this discrepancy to the uncertainties related to ^{14}C-dating of bulk material. The third sample
490   from the southern trench wall, SLO18_SK6, was a charcoal from unit U10 and returned an age of 2440 - 2315 cal BP. This is
older than unit U5, but similar to the bulk sample from the fissure fill. However, the history of that charcoal is unknown. It
might have been washed-in after it spent some time in a sediment reservoir upstream. The most conservative interpretation of
the dating results from the southern trench wall is that the deformation occurred after 2067 cal BP, that is, the emplacement of
U5.
495   Taking the results from both trench walls together leads us to conclude that the observed deformation can be bracketed to 2140
- 315 cal BP. This time span would allow the 1511 Idrija Earthquake to be the causative event. Arguments in favour of this

interpretation are the destruction of the town of Idrija in 1511, which could be explained by a fault rupture in the vicinity of the present-day city, and the results of Bavec et al. (2013) who trenched the fault close to our site (Fig. 6) and found evidence for deformation dating to about 900 - 360 cal BP. Arguments against the 1511 earthquake as the causative event come from
500   the trench by Falcucci et al. (2018). These authors found evidence for 16th century ruptures on a fault in Italy that fits the macroseismic damage pattern. However, this does not exclude the possibility of surface ruptures near Idrija. Some authors note that in 1511 two faults may have ruptured in close succession, based on different times reported in the Italian and Slovenian historical documents and on the bimodal distribution of shaking (Ribarič, 1979). However, Cecić (2011) and Camassi et al. (2011) summarise the evidence for a calculation error in the occurrence times and conclude that the historical
505   reports do not require two events. Another argument against the 1511 earthquake as the causative event for the ruptures observed in our trench is the lack of descriptions of surface ruptures near Idrija. However, this argument is weak because of the general uncertainty of historical sources. On the one hand, many trained engineers and geologists were in Idrija in 1511 because of the mercury mine, and they could have contributed detailed geological observations if there had been surface ruptures. On the other hand, all their post-earthquake efforts were probably concentrated on repairing the mine, which was one
510   of the most important enterprises in the entire region back then.

5.5 Earthquake magnitude on the Idrija Fault

We have only few constraints on the magnitude of the paleo-earthquake on the Idrija Fault. Based on the arguments in section 5.3, we interpret the observed deformation features as primary effects (sensu Michetti et al., 2007; Guerrieri, 2015) due to the coseismic offsets, not as secondary effects caused by strong ground motion. We were not able to measure offsets in the trench,
515   because we did not undertake 3D trenching. Following a similar line of reasoning as with the Predjama Fault earthquakes, an earthquake that caused a surface rupture is likely to have been stronger than the historical earthquakes in the region, which presumably caused no surface ruptures. Both the magnitude (M6.8-6.9, Ribarič, 1979; Fitzko et al., 2005) and the timing of the 1511 Idrija Earthquake would fit our observations. However, several 20th century strike-slip earthquakes with lower magnitudes caused surface ruptures, too (Wells and Coppersmith, 1994; Stirling et al., 2002). If the entire Idrija Fault ruptured
520   in one earthquake, the empirical relationships of Wells and Coppersmith (1994) and Leonard (2010) for strike-slip earthquakes would allow for a magnitude of M_W7.5-7.6. An earthquake this size would very likely cause several metres of surface displacement. Although we cannot quantify the offset in our trench, we suspect that such large displacements would still be visible elsewhere along the fault. Thus, we conservatively conclude that the Idrija Fault has caused a surface rupturing earthquake with a magnitude probably greater than M_W6.1.

525   **5.6 Implications for regional tectonics and seismic hazard**

Holocene surface rupturing earthquakes on the NW-SE trending faults in the area have been proven for the Colle Villano Thrust on the mountain front in Italy (Falcucci et al., 2018), for the Predjama Fault (this study), and for the Idrija Fault (Bavec et al., 2013; this study). Historical earthquakes on the Idrija Fault and in the Ljubljana Basin exceeded M_W6.0 (e.g., Ribarič,

530 1982; Fitzko et al., 2005; Cecić, 2015). Instrumental earthquakes on the Ravne Fault had magnitudes of $M_S5.7$ and $M_W5.2$ (Bajc et al., 2001; Kastelic et al., 2004, 2008). These observations indicate that the crustal deformation due to the northward motion of Adria is not localised and that the long time-averaged seismic moment release is probably more widely distributed than previously estimated from historical and instrumental data (Serpelloni et al., 2016).
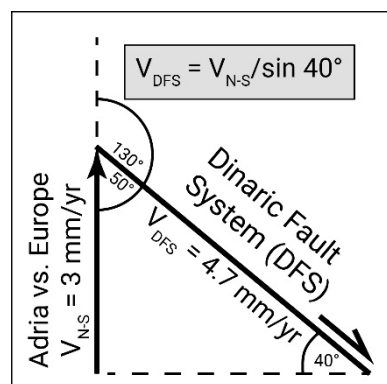
Figure 8: Simple slip-rate estimation for the DFS in Western Slovenia. A northward velocity of Adria with respect to Europe of
535 **3 mm/yr (Weber et al., 2010) would lead to 4.7 mm/yr of right-lateral strike-slip on the Dinaric Fault System if this were the only way of accommodating the deformation. Hence, the combined slip rates of the DFS cannot exceed 4.7 mm/yr.**

The GPS velocity of Adria with respect to stable Eurasia is 3 mm/yr (Weber et al., 2010). If the entire northward motion of Adria were accommodated by the right-lateral motion on the DFS striking ~130°, the summed slip rate would be 4.7 mm/yr (Fig. 8). However, Moulin et al. (2016) also report folding from the Čepovan Canyon area as a result of the transpressive
540 regime, and other means of deformation such as block rotations about vertical axes cannot be ruled out. Hence, the 4.7 mm/yr of cumulative slip rate of the DFS must be regarded as a maximum, of which the Periadriatic Fault System alone takes up at least 1 mm/yr (Vrabec et al., 2006). As a result, none of the active faults of the DFS can be expected to have slip-rates exceeding c. 1.4 to 2.1 mm/yr. The measured shortening is accommodated by a series of active faults, whose slip-rates estimations vary between 0.05-2.0 mm/yr according to the available data (Kastelic and Carafa, 2012; Atanackov et al., 2016; Moulin et al.,
545 2016). The DFS with the main Idrija, Predjama, and Raša faults accommodates the majority of shortening in western Slovenia (Atanackov et al., 2016; Moulin et al., 2016). Neither our study nor the paleoseismological investigations by Bavec et al. (2013) and Falcucci et al. (2018) revealed evidence for short earthquake recurrence intervals. At the Predjama Fault, we have found at least one earthquake in the past 13 ka, more likely within the past 8.4 ka. For the Idrija Fault, only one earthquake could be proven for the last 2 ka (Bavec et al., 2013, this study). Falcucci et al. (2018) document three ruptures on the Colle
550 Villano Thrust. The oldest one pre-dates 7 ka, the two younger ones happened probably after the 6th century AD. This evidence for large, but rare events further supports the argument for low fault slip-rates.

Vičič et al. (2019) reported earthquake swarms on the NW-SE striking strike-slip faults in Slovenia. On the southern Predjama Fault, more than 3000 earthquakes occurred between late 2009 and early 2011. The strongest event was $M_L3.5$ and had a predominant strike-slip mechanism. This swarm was accompanied by a transient recorded by an extensometer in Postojna
555 Cave. The transient deformation was a few hundreds of a millimetre only. No earthquake swarm occurred near our trench site.

However, this raises the question if creep or slow-slip events along the NW-SE faults can release a significant part of the seismic moment. In our trench across the Predjama fault, we found evidence for rapid deformation only, which means that the fault is at least partly, perhaps entirely, locked. Another earthquake swarm on the Idrija Fault NW of our trench site was reported by Vičič et al. (2019), but no swarms occurred at our study site. Vičič et al. (2019) investigated a possible driving

560   mechanism for the swarms and conclude that a slow slip event on the deeper part of the southern Idrija fault (deeper than 18 km) could explain the increased microseismic activity. The shallower part of the Idrija Fault in our study area is locked, as indicated by the structures we found in our trench and by the lack of instrumental seismicity over the period of 1977-2010 reported by Živčić et al. (2011).

From a seismic hazard perspective, it must be assumed that all of the large NW-SE tending strike-slip faults could rupture in

565   a strong earthquake at any time, although recurrence intervals on the individual faults are large. Thus, instrumental seismicity and even historical data may not adequately depict the actual hazard.

6 Conclusions

With a combination of geomorphological investigations, near-surface geophysical surveys, and paleoseismological trenching we show that surface-rupturing earthquakes happened on the Predjama and Idrija Faults in western Slovenia in the Holocene.

570   At least one earthquake on the Predjama Fault resulted in a vertical displacement of ~0.5 m and an unknown amount of horizontal offset. A minimum magnitude of $M_W6.1$ is necessary to cause the observed deformation. We can reliably bracket the event to an age of 13 - 0.7 ka. However, the good agreement of several radiocarbon samples indicates that the deformation more likely happened not earlier than 8.4 ka. The Idrija Fault had an earthquake of at least magnitude $M_W6.1$ in the last ~2.1 ka. This earthquake displaced fluvial sediments and caused an open fissure which was then re-filled. Our dating results would

575   allow this event to be the 1511 Idrija Earthquake, but the evidence for that is not conclusive. Since several active faults share the geodesy-derived 3 mm/yr of relative motion between Adria and Eurasia, none of them can have a high slip rate. These faults rupture in strong, but rare earthquakes, which likely dominate the overall seismic moment release on the NW-SE trending strike-slip faults in the study area. The results of our study show that Holocene earthquakes on the two faults exceeded the magnitudes in the instrumental earthquake catalogue. A seismic hazard assessment solely based on instrumental and historical

580   data would miss the strongest possible events.

Author contribution

CG, KR, and KU designed the study. JW and CG undertook the remote sensing research. CG led the field investigations. SA, NS, JW, BV, PJR, MV, and CG ran the field campaign. SA and NS analysed the geophysics results. CG compiled the data and wrote the initial draft of the manuscript. All authors reviewed and edited the first draft.

585 **Competing interests**

The authors declare that they have no conflict of interest.

Acknowledgements

This study was undertaken in the framework of SPP 2017 – Mountain Building Processes in 4D. We thank our field crew
Alexander Krämer, Andrea Viscolani, Hamid Sana, and Wahid Abbas for their support. This work benefitted from discussions
590 with Jure Atanackov, Jernej Jež, and Tomaž Fabec, who also provided a 19th century cadaster plan from the Banjšice site.
Elena Makorič (Pokrajinski arhiv v Novi Gorici) is thanked for finding the historical photographs from World War I. SRTM
data are distributed by the Land Processes Distributed Active Archive Center (LPDAAC), located at USGS/EROS, Sioux
Falls, SD, http://lpdaac.usgs.gov. Slovenian LiDAR data are provided by Ministry of the Environment and Spatial Planning,
Slovenian Environment Agency (ARSO). CG is financed by the DFG, project numbers GR 4371/1-1 and GR 4371/3-1 (SPP
595 2017 – Mountain Building Processes in 4D). PJR is financed by ARRS program P1—0011 (Regional Geology).

References

Agosta, F., Ruano, P., Rustichelli, A., Tondi, E., Galindo-Zaldívar, J. and de Galdeano, C. S.: Inner structure and deformation
mechanisms of normal faults in conglomerates and carbonate grainstones (Granada Basin, Betic Cordillera, Spain): Inferences
on fault permeability. Journal of Structural Geology, 45, 4-20, 2012.

600 AHEAD Working Group: AHEAD, the European Archive of Historical Earthquake Data. https://doi.org/10.6092/INGV.IT-
AHEAD, accessed on 2020-07-16, 2020.

Alfaro, P., Galindo-Zaldívar, J., Jabaloy, A., López-Garrido, A. C. and de Galdeano, C. S.: Evidence for the activity and
paleoseismicity of the Padul fault (Betic Cordillera, southern Spain). Acta geológica hispánica, 36(3), 283-295, 2001.

Anderson, H. A. and Jackson, J. A.: Active tectonics of the Adriatic region. Geophys. J. R. Astron. Soc., 91, 937–983,
605 doi:10.1111/j.1365-246X.1987.tb01675.x., 1987.

Aoudia, A., Saraò, A., Bukchin, B. and Suhadolc, P.: The 1976 Friuli (NE Italy) thrust faulting earthquake: a reappraisal 23
years later, Geophys. Res. Lett., 27(4), 573–576, 2000.

Atanackov, J., Jamšek Rupnik, P., Jež, J., Milanič, B., Novak, M., Celarc, B., Markelj, A. and Bavec, M.: Database of active
faults in Slovenia. In Procedings of the 7th International INQUA Meeting on Paleoseismology, Active Tectonics and
610 Arheoseismology. Crestone, 5-8. 2016

Atwater, B. F.: Geologic evidence for earthquakes during the past 2000 years along the Copalis River, southern coastal
Washington. Journal of Geophysical Research: Solid Earth, 97(B2), 1901-1919, 1992.

Audemard, F. A.: Surface rupture of the Cariaco July 09, 1997 earthquake on the El Pilar fault, northeastern Venezuela.
Tectonophysics, 424(1-2), 19-39, 2006.

615   Bajc, J., Aoudia, A., Saraó, A., and Suhadolc, P: The 1998 Bovec-Krn Mountain (Slovenia) Earthquake Sequence. Geophysical Research Letters, 28(9), 1839-1842, 2001.

Barrell, D. J. A., Litchfield, N. J., Townsend, D. B., Quigley, M., Van Dissen, R. J., Cosgrove, R., Cox, S.C., Furlong, K., Villamor, P., Begg, J.G., Hemmings-Sykes, S., Jongens, R., Mackenzie, H., Noble, D., Stahl, T., Bilderback, E., Duffy, B., Henham, H., Klahn, A., Lang, E.M.W., Moody, L., Nicol, R., Pedley, K., and Smith, A.: Strike-slip ground-surface rupture

620   (Greendale Fault) associated with the 4 September 2010 Darfield earthquake, Canterbury, New Zealand. Quarterly Journal of Engineering Geology and Hydrogeology, 44(3), 283-291, 2011.

Bavec, M., Car, M., Stopar, R., Jamšek, P., and Gosar, A.: Geophysical evidence of recent activity of the Idrija fault, Kanomlja, NW Slovenia. Materials and Geoenvironment, 59, 247-256, 2012.

Bavec, M., Atanackov, J., Celarc, B., Hajdas, I., Jamšek Rupnik, P., Jež, J., Kastelic, V., Milanič, B., Novak, M., Skaberne,

625   G. and Žibret, G.: Evidence of Idrija fault seismogenic activity during the Late Holocene including the 1511 Mm 6.8 earthquake. In C. Grützner, A. Rudersdorf, R. Pérez-López & K. Reicherter (eds.): Proceedings of the 4th International INQUA Meeting on Paleoseismology, Active Tectonics and Archeoseismology (PATA), 9-14 October 2013, Aachen, 23-26, ISBN: 978-3-00-042796-1, 2013.

Bertran, P., Manchuel, K. and Sicilia, D.: Discussion on 'Palaeoseismic structures in Quaternary sediments, related to an

630   assumed fault zone north of the Permian Peissen-Gnutz salt structure (NW Germany)–Neotectonic activity and earthquakes from the Saalian to the Holocene'(Grube, 2019). Geomorphology, 365, 106704, 2020.

Bronk Ramsey, C.: Bayesian analysis of radiocarbon dates. Radiocarbon, 51(1), 337-360, 2009.

Calais, E., Nocquet, J.M., Jouanne, F., and Tardy, M.: Current strain regime in the Western Alps from continuous Global Positioning System measurements. Geology 30, 651–654, doi: 10.1130/0091-7613(2002)030<0651:CSRITW>2.0.CO;2,

635   2002.

Camassi, R., Caracciolo, C.H., Castelli, V. and Slejko, D.: The 1511 Eastern Alps earthquakes: a critical update and comparison of existing macroseismic datasets, J. Seismol., 15, 191-213, 2011.

Čar, J.: Geological structure of the Idrija - Cerkno hills: Explanatory book to the Geological map of the Idrija - Cerkljansko hills between Stopnik and Rovte 1: 25 000. Geological survey of Slovenija, Ljubljana, 2010.

640   Čarman, M., Živčić, M. and Ložar Stopar, M.: Earthquakes Near Ilirska Bistrica in 2010. Earthquakes in 2010. ARSO, 2011.

Cecić, I.: Idrijski potres 26. marca 1511 – kaj pravzaprav vemo o njem? [The 26 March 1511 earthquake – What do we know about it?]. Geografski obzornik 58(1):24–29, 2011.

Cecić, I.: Earthquakes in Tuhinj Valley (Slovenia) In 1840. Journal of Seismology, 19(2), 469-490, 2015.

Champenois, J., Baize, S., Vallée, M., Jomard, H., Alvarado, A., Espin, P., Ekström, G. and Audin, L.: Evidences of surface

645   rupture associated with a low-magnitude (M w 5.0) shallow earthquake in the Ecuadorian Andes. Journal of Geophysical Research: Solid Earth, 122(10), 8446-8458, 2017.

Choi, J. H., Klinger, Y., Ferry, M., Ritz, J. F., Kurtz, R., Rizza, M., Bollinger, L., Davaasambuu, B., Tsend-Ayush, N. and Demberel, S.: Geologic inheritance and earthquake rupture processes: The 1905 M≥ 8 Tsetserleg-Bulnay strike-slip earthquake sequence, Mongolia. Journal of Geophysical Research: Solid Earth, 123(2), 1925-1953, 2018.

650 Copley, A., Grützner, C., Howell, A., Jackson, J., Penney, C. and Wimpenny, S: Unexpected earthquake hazard revealed by Holocene rupture on the Kenchreai Fault (central Greece): Implications for weak sub-fault shear zones. Earth and Planetary Science Letters 486, 141-154, 2018.

Cubrinovski, M., Robinson, K., Taylor, M., Hughes, M. and Orense, R.: Lateral spreading and its impacts in urban areas in the 2010–2011 Christchurch earthquakes. New Zealand Journal of Geology and Geophysics, 55(3), 255-269, 2012.

655 Cunningham, D., Grebby, S., Tansey, K., Gosar, A., and Kastelic, V.: Application of airborne LiDAR to mapping seismogenic faults in forested mountainous terrain, southeastern Alps, Slovenia. Geophysical Research Letters, 33(20), 2006.

Cunningham, D., Gosar, A., Kastelic, V., Grebby, S., and Tansey, K.: Multi-disciplinary investigations of active faults in the Julian Alps, Slovenia. Acta Geodynamica et Geomaterialia, 4(1), 2007.

D'Agostino, N., Cheloni, D., Mantenuto, S., Selvaggi, G., Michelini, A., and Zuliani, D.: Strain accumulation in the southern
660 Alps (NE Italy) and deformation at the northeastern boundary of Adria observed by CGPS measurements. Geophysical Research Letters, 32(19), L19306, doi:10.1029/2005GL024266, 2005.

D'Agostino, N., Avallone, A., Cheloni, D., D'Anastasio, E., Mantenuto, S., and Selvaggi, G.: Active tectonics of the Adriatic region from GPS and earthquake slip vectors. JGR: Solid Earth, 113, B12413, doi:10.1029/2008JB005860, 2008.

Duman, T. Y., Emre, O., Dogan, A. and Ozalp, S.: Step-over and bend structures along the 1999 Duzce earthquake surface
665 rupture, North Anatolian fault, Turkey. Bulletin of the Seismological Society of America, 95(4), 1250-1262, 2005.

Eidelman, A. and Reches, Z. E.: Fractured pebbles—A new stress indicator. Geology, 20(4), 307-310, 1992.

England, P. and Jackson, J.: Uncharted seismic risk. Nature Geoscience, 4, 348–349, doi:10.1038/ngeo1168, 2011.

Falcucci, E., Eliana Poli, M., Galadini, F., Scardia, G., Paiero, G., and Zanferrari, A.: First evidence of active transpressive surface faulting at the front of the eastern Southern Alps, northeastern Italy: insight on the 1511 earthquake seismotectonics.
670 Solid Earth, 911-922, doi:10.5194/se-9-911-2018, 2018.

Fitzko, F., Suhadolc, P., Aoudia, A., and Panza, G. F.: Constraints on the location and mechanism of the 1511 Western-Slovenia earthquake from active tectonics and modeling of macroseismic data. Tectonophysics, 404(1-2), 77-90, doi: 10.1016/j.tecto.2005.05.003, 2005.

Ghose, S., Mellors, R. J., Korjenkov, A. M., Hamburger, M. W., Pavlis, T. L., Pavlis, G. L., Omuraliev, M., Mamyrov, E., and
675 Muraliev, A. R.: The MS= 7.3 1992 Suusamyr, Kyrgyzstan, earthquake in the Tien Shan: 2. Aftershock focal mechanisms and surface deformation. Bulletin of the Seismological Society of America, 87(1), 23-38, 1997.

Glaise von Horstenau, E.: Österreich-Ungarns letzter Krieg 1914 - 1918. Vol. 6 - Das Kriegsjahr 1917. Verl. der Militärwiss. Mitteilungen, Vienna, Austria, 1932.

Gosar, A., Šebela, S., Košťák, B. and Stemberk, J.: On the state of the TM 71 extensometer monitoring in Slovenia: seven
680 years of micro-tectonic displacement measurements. Acta geodynamica et geomaterialia 8, 4: 389–402, 2011

Grünthal, G., Wahlström, R., and Stromeyer, D.: The SHARE European Earthquake Catalogue (SHEEC) for the time period 1900–2006 and its comparison to the European-Mediterranean Earthquake Catalogue (EMEC). J Seismology, 17(4), 1339-1344, doi:10.1007/s10950-013-9379-y, 2013.

685 Grützner, C., Aschenbrenner, S., Krämer, A., Reicherter, K., Saifelislam, N., Ustaszewski, K., Viscolani, A., and Welte, J.: Geophysical survey (GPR, ERT, magnetic) on active faults in Slovenia and Italy. PANGAEA, https://doi.pangaea.de/10.1594/PANGAEA.922902, 2020.

Guerrieri, L. (ed): Earthquake Environmental Effect for seismic hazard assessment: the ESI intensity scale and the EEE Catalogue. Memorie Descrittive Della Carta Geologica D'Italia 97, 2015.

Handy, R.M., Ustaszewski, K. and Kissling, E.: Reconstructing the Alps-Carpathians-Dinarides as a key to understanding 690 switches in subduction polarity, slab gaps and surface motion. Int. J. Earth Sci., 104, 1–26. doi: 10.1007/s0053101410603, 2015.

Hayes, G. P., Briggs, R. W., Sladen, A., Fielding, E. J., Prentice, C., Hudnut, K., Mann, P., Taylor, F. W., Crone, A. J., Gold, R. and Ito, T.: Complex rupture during the 12 January 2010 Haiti earthquake. Nature Geoscience, 3(11), 800-805, 2010

Herak, M., Herak, D., and Markušić, S.: Fault plane solutions for earthquakes (1956-1995) in Croatia and neighboring regions. 695 Geofizika, 12(1), 43-56, 1995.

Herak, D., Herak, M., and Tomljenović, B.: Seismicity and earthquake focal mechanisms in North-Western Croatia. Tectonophysics 465, no. 1-4, 212-220, 2009.

Herak, D., Sović, I., Cecić, I., Živčić, M., Dasović, I., and Herak, M.: Historical seismicity of the Rijeka region (northwest external Dinarides, Croatia)—Part I: Earthquakes of 1750, 1838, and 1904 in the Bakar epicentral area. Seismol Res Lett, 700 88(3), 904-915, 2017.

Herak, M., Živčić, M., Sović, I., Cecić, I., Dasović, I., Stipčević, J., and Herak, D.: Historical Seismicity of the Rijeka Region (Northwest External Dinarides, Croatia)—Part II: The Klana Earthquakes of 1870. Seismol Res Lett, 89(4), 1524-1536, 2018.

Hooyer, T. S. and Iverson, N. R.: Clast-fabric development in a shearing granular material: implications for subglacial till and fault gouge. Geological Society of America Bulletin, 112(5), 683-692, 2000.

705 Howarth, J. D., Cochran, U. A., Langridge, R. M., Clark, K., Fitzsimons, S. J., Berryman, K., Villamor, P. and Strong, D. T.: Past large earthquakes on the Alpine Fault: Paleoseismological progress and future directions. New Zealand Journal of Geology and Geophysics, 61(3), 309-328, 2018.

Jamšek Rupnik, P., Živčić, M., Atanackov, J., Celarc, B., Jež, J., Novak, M., Milanič, B., Jesenko, T., Ložar Stopar, M. and Bavec, M.: Seismotectonic map. In: Novak, M. and Rman, N. (ed). Geological atlas of Slovenia. Ljubljana: Geological Survey 710 of Slovenia. 2016, p. 96-97, 2016.

Kastelic, V. and Carafa, M. M. C.: Fault slip rates for the active external Dinarides thrust-and-fold belt. Tectonics 31. doi:10.1029/2011TC003022, 2012.

Kastelic, V., Živčić, M., Pahor, J., and Gosar, A.: Seismotectonic characteristics of the 2004 earthquake in Krn mountains. Potresi v letu 2004, ARSO, Ljubljana, 78-87, 2004.

715   Kastelic, V., Vrabec, M., Cunningham, D., and Gosar, A.: Neo-Alpine structural evolution and present-day tectonic activity of the eastern Southern Alps: The case of the Ravne Fault, NW Slovenia. J Struct Geol, 30(8), 963-975, 2008.

Landgraf, A., Kübler, S., Hintersberger, E., and Stein, S.: Active tectonics, earthquakes and palaeoseismicity in slowly deforming continents. Geological Society, London, Special Publications, 432(1), 1-12, doi:10.1144/SP432.13, 2017.

Langridge, R. M., Villamor, P., Howarth, J. D., Ries, W. F., Clark, K. J. and Litchfield, N. J.: Reconciling an Early Nineteenth-

720   Century Rupture of the Alpine Fault at a Section End, Toaroha River, Westland, New Zealand. Bulletin of the Seismological Society of America, doi:10.1785/0120200116, 2020.

Leonard, M.: Earthquake fault scaling: Self-consistent relating of rupture length, width, average displacement, and moment release. Bulletin of the Seismological Society of America, 100(5A), 1971-1988, 2010.

McNeill, L. C., Collier, R. L., De Martini, P. M., Pantosti, D. and D'Addezio, G.: Recent history of the Eastern Eliki Fault,

725   Gulf of Corinth: geomorphology, palaeoseismology and impact on palaeoenvironments. Geophysical Journal International, 161(1), 154-166, 2005.

Metois, M., D'Agostino, N., Avallone, A., Chamot-Rooke, N., Rabaute, A., Duni, L., Kuka, N., Koci, R. and Georgiev, I.: Insights on continental collisional processes from GPS data: Dynamics of the peri-Adriatic belts. Journal of Geophysical Research: Solid Earth, 120(12), 8701-8719, 2015.

730   Michetti, A.M., Esposito, E., Guerrieri, L., Porfido, S., Serva, L., Tatevossian, R., Vittori, E., Audemard, F., Azuma, T., Clague, J., et al.: Intensity scale ESI 2007. In: Memorie Descrittive Carta Geologica d'Italia. Servizio Geologico d'Italia; Guerrieri, L., Vittori, E., Eds.; 74. Dipartimento Difesa del Suolo, APAT: Rome, Italy; Volume 74, p. 53, 2007.

Moulin, A., Benedetti, L., Gosar, A., Jamšek Rupnik, P., Rizza, M., Bourlès, D., and Ritz, J. F.: Determining the present-day kinematics of the Idrija fault (Slovenia) from airborne LiDAR topography. Tectonophysics, 628, 188-205, 2014.

735   Moulin, A., Benedetti, L., Rizza, M., Jamšek Rupnik, P., Gosar, A., Bourles, D., Keddadouche, K., Aumaître, G., Arnold, M., Guillou, V., and Ritz, J. F.: The Dinaric fault system: Large-scale structure, rates of slip, and Plio-Pleistocene evolution of the transpressive northeastern boundary of the Adria microplate. Tectonics, 35(10), 2258-2292, doi:10.1002/2016TC004188, 2016.

Papathanassiou, G. and Pavlides, S.: Using the INQUA scale for the assessment of intensity: Case study of the 2003 Lefkada

740   (Ionian Islands), Greece earthquake. Quaternary International, 173, 4-14, 2007.

Patyniak, M., Landgraf, A., Dzhumabaeva, A., Abdrakhmatov, K. E., Rosenwinkel, S., Korup, O., Preusser, F., Fohlmeister, J., Arrowsmith, J. R. and Strecker, M. R.: Paleoseismic Record of Three Holocene Earthquakes Rupturing the Issyk-Ata Fault near Bishkek, North KyrgyzstanPaleoseismic Record of Three Holocene Earthquakes Rupturing the Issyk-Ata Fault near Bishkek. Bulletin of the Seismological Society of America, 107(6), 2721-2737, 2017.

745   Peruzza, L., Poli, M.E., Rebez, A., Renner, G., Rogledi, S., Slejko, D. and Zanferrari, A.: The 1976–1977 seismic sequence in Friuli: new seismotectonic aspects, Mem. Soc. Geol. It., 57, 391–400, 2002.

Placer, L.: Structural history of the Idrija mercury deposit, Geologija, 25/1, 7–94, 1982.

Placer, L., Vrabec, M., and Celarc, B.: The bases for understanding of the NW Dinarides and Istria Peninsula tectonics. Geologija, 53(1), 55-86, doi:10.5474/geologija.2010.005, 2010.

750 Poljak, M., Živčić, M. and Zupančič, P.: The seismotectonic characteristics of Slovenia. Pure and Applied Geophysics 157(1–2), 37–55, 2000.

Pondrelli, S., Morelli, A., Ekström, G., Mazza, S., Boschi, E., and Dziewonski, A. M.: European-Mediterranean regional centroid-moment tensors: 1997-2000. Phys. Earth Planet. Int., 130, 71-101, doi:10.1016/S0031-9201(01)00312-0, 2002.

Pondrelli, S., Salimbeni, S., Morelli, A., Ekström, G., Postpischl, L., Vannucci, G., and Boschi, E.: European–Mediterranean

755 regional centroid moment tensor catalog: solutions for 2005–2008. Phys. Earth Planet. Int., 185(3-4), 74-81, 2011.

Radjai, F., Wolf, D. E., Jean, M. and Moreau, J. J.: Bimodal character of stress transmission in granular packings. Physical review letters, 80(1), 61, 1998.

Ramsay, D. M.: Deformation of pebbles in lower Old Red Sandstone conglomerates adjacent to the Highland Boundary fault. Geological Magazine, 101(3), 228-248, 1964.

760 Reimer, P.J., Bard, E., Bayliss, A., Beck, J.W., Blackwell, P.G., Bronk Ramsey, C., Buck, C.E., Cheng, H., Edwards, R.L., Friedrich, M., Grootes, P.M., Guilderson, T.P., Hafl-idason, H., Hajdas, I., Hatté, C., Heaton, T.J., Hoffmann, D.L., Hogg, A.G., Hughen, K.A., Kaiser, K.F., Kromer, B., Manning, S.W., Niu, M., Reimer, R.W., Richards, D.A., Scott, E.M., Southon, J.R., Staff, R.A., Turney, C.S.M., and van der Plicht, J.: IntCal13 and Marine13 radiocarbon age calibration curves 0–50,000 years cal BP. Radiocarbon, 55(4), 1869-1887, 2013.

765 Ribarič, V.: The Idrija earthquake of March 26, 1511—a reconstruction of some seismological parameters. Tectonophysics, 53(3-4), 315-324, 1979.

Ribarič, V.: Seismicity of Slovenia-Catalogue of Earthquakes (792 A.D-I98I), SZ SRS, Publication, Ser. A, No. I-I, Ljubljana, 650 pp., 1982.

Ritz, J. F., Baize, S., Ferry, M., Larroque, C., Audin, L., Delouis, B., and Mathot, E.: Surface rupture and shallow fault

770 reactivation during the 2019 Mw 4.9 Le Teil earthquake, France. Communications Earth & Environment, 1(1), 1-11, 2020.

Sapkota, S. N., Bollinger, L., Klinger, Y., Tapponnier, P., Gaudemer, Y. and Tiwari, D.: Primary surface ruptures of the great Himalayan earthquakes in 1934 and 1255. Nature Geoscience, 6(1), 71-76, 2013.

Schmid, S.M., Bernoulli, D., Fügenschuh, B., Matenco, L., Schefer, S., Schuster, R., Tischler, M. and Ustaszewski, K.: The Alpine-Carpathian-Dinaridic orogenic system: correlation and evolution of tectonic units. Swiss J. Geosci., 101, 139–183. doi:

775 10.1007/s0001500812473, 2008.

Serpelloni, E., Vannucci, G., Anderlini, L. and Bennett, R. A.: Kinematics, seismotectonics and seismic potential of the eastern sector of the European Alps from GPS and seismic deformation data. Tectonophysics, 688, 157-181, 2016

Silva, P. G., Reicherter, K., Grützner, C., Bardají, T., Lario, J., Goy, J. L., Zazo, C. and Becker-Heidmann, P.: Surface and subsurface palaeoseismic records at the ancient Roman city of Baelo Claudia and the Bolonia Bay area, Cádiz (south Spain).

780 Geological Society, London, Special Publications, 316(1), 93-121, 2009.

Slejko, D., Carulli, G. B., Nicolich, R., Rebez, A., Zanferrari, A., Cavallin, A., Doglioni, C., Carraro, F., Castaldini, D., Iliceto, V., Semenza, E. and Zanolla, C.: Seismotectonics of the Eastern Southern Alps: a review. Boletino di Geofisica Teorica ed Applicata, 31(122), 109-136, 1989.

Stein, S., Liu, M., Calais, E. and Li Q.: Mid-continent earthquakes as a complex system. Seismol Res Lett, 80, 551–553, doi:10.1785/gssrl.80.4.551, 2009.

Stirling, M., Rhoades, D. and Berryman, K.: Comparison of earthquake scaling relations derived from data of the instrumental and preinstrumental era. Bulletin of the Seismological Society of America, 92(2), 812-830, 2002.

Stucchi, M., Rovida, A., Capera, A. G., Alexandre, P., Camelbeeck, T., Demircioglu, M. B., Gasperini, P., Kouskouna, V., Musson, R. M. W., Radulian, M., Sesetyan, K., Vilanova, S., Baumont, D., Bungum, H., Fäh, D., Lenhardt, W., Makropoulos, K., Martinez Solares, J. M., Scotti, O., Živčić, M., Albini, P., Batllo, J., Papaioannou, C., Tatevossian, R., Locati, M., Meletti, C., Viganò, D., and Giardini, D.: The SHARE European earthquake catalogue (SHEEC) 1000–1899. J Seismology, 17(2), 523-544, doi:10.1007/s10950-012-9335-2, 2013.

Sylvester, A. G.: Strike-slip faults. Geological Society of America Bulletin, 100(11), 1666-1703, 1988.

Talebian, M., Fielding, E. J., Funning, G. J., Ghorashi, M., Jackson, J., Nazari, H., Parsons, B., Priestley, K., Rosen, P. A., Walker, R. and Wright, T. J.: The 2003 Bam (Iran) earthquake: Rupture of a blind strike-slip fault. Geophysical research letters, 31(11), 2004.

Thakur, V. C. and Pandey, A. K.: Late Quaternary tectonic evolution of Dun in fault bend/propagated fold system, Garhwal Sub-Himalaya. Curr. Sci, 87(11), 1567-1576, 2004.

Tiberi, L., Costa, G., Jamšek Rupnik, P., Cecić, I. and Suhadolc, P.: The 1895 Ljubljana earthquake: can the intensity data points discriminate which one of the nearby faults was the causative one? Journal of Seismology, 22, 927–941. doi.org/10.1007/s10950-018-9743-z, 2018.

Tokarski, A. K. and Strzelecki, P. J.: Fractured clasts in the Mt Currie Conglomerate at Kata Tjuta (Central Australia): evidence of Early Cambrian earthquakes?. Geology, Geophysics and Environment, 46(1), 29, 2020.

Tokarski, A. K., Świerczewska, A., Lasocki, S., Cuong, N. Q., Strzelecki, P. J., Olszak, J., Kukulak, J., Alexanderson, H., Zasadni, J., Krąpiec, M. and Mikołajczak, M.: Active faulting and seismic hazard in the Outer Western Carpathians (Polish Galicia): Evidence from fractured Quaternary gravels. Journal of Structural Geology, 141, 104210, 2020.

Treiman, J. A., Kendrick, K. J., Bryant, W. A., Rockwell, T. K. and McGill, S. F.: Primary surface rupture associated with the M w 7.1 16 October 1999 Hector Mine earthquake, San Bernardino County, California. Bulletin of the Seismological Society of America, 92(4), 1171-1191, 2002.

Ustaszewski, K., Kounov, A., Schmid, S.M., Schaltegger, U., Krenn, E., Frank, W. and Fügeschuh, B.: Evolution of the Adria-Europe plate boundary in the northern Dinarides: From continent-continent collision to backarc extension. Tectonics, 29, 1–34. doi:10.1029/2010TC002668, 2010.

Valjavec, M. B., Zorn, M., and Ribeiro, D.: Mapping war geoheritage: Recognising geomorphological traces of war. Open Geosciences, 10(1), 385-394, 2018.

815 Vanneste, K. and Verbeeck, K.: Paleoseismological analysis of the Rurrand fault near Julich, Roer Valley graben, Germany: Coseismic or aseismic faulting history?. Geologie en Mijnbouw, 80(3/4), 155-170, 2001.

Vičič, B., Aoudia, A., Javed, F., Foroutan, M., and Costa, G.: Geometry and mechanics of the active fault system in western Slovenia. Geophys. J. Int., 217, 1755–1766, 2019.

Vrabec, M. and Fodor, L.: Late Cenozoic tectonics of Slovenia: structural styles at the Northeastern corner of the Adriatic
820 microplate" in The Adria microplate: GNSS geodesy, tectonics and hazards (NATO Science Series IV, Earth and Environmental Sciences 61), eds. N. Pinter, N. Grenerczy, J. Weber, S. Stein, D. Medak (Dordrecht, Springer), 151–168, 2006.

Wang, Y., Amundson, R. and Trumbore, S.: Radiocarbon dating of soil organic matter. Quaternary Research, 45(3), 282-288, 1996.

Vrabec, M., Preseren, P. P. and Stopar, B.: GPS study (1996-2002) of active deformation along the Periadriatic fault system
825 in northeastern Slovenia: tectonic model. Geologica Carpathica-Bratislava, 57(1), 57-65, 2006.

Weber, J., Vrabec, M., Pavlovčič-Prešeren, P., Dixon, T., Jiang, Y., and Stopar, B.: GPS-derived motion of the Adriatic microplate from Istria Peninsula and Po Plain sites, and geodynamic implications. Tectonophysics, 483(3), 214-222, doi:10.1016/j.tecto.2009.09.001, 2010.

Wells, D. L., & Coppersmith, K. J.: New empirical relationships among magnitude, rupture length, rupture width, rupture area,
830 and surface displacement. Bulletin of the seismological Society of America, 84(4), 974-1002, 1994.

Zabcı, C., Akyüz, H. S. and Sançar, T.: Palaeoseismic history of the eastern part of the North Anatolian Fault (Erzincan, Turkey): Implications for the seismicity of the Yedisu seismic gap. Journal of Seismology, 21(6), 1407-1425, 2017.

Zachariasen, J., Berryman, K., Langridge, R., Prentice, C., Rymer, M., Stirling, M. and Villamor, P.: Timing of late Holocene surface rupture of the Wairau fault, Marlborough, New Zealand. New Zealand Journal of Geology and Geophysics, 49(1),
835 159-174, 2006.

Žibret, L. and Vrabec, M.:. Paleostress and kinematic evolution of the orogen-parallel NW-SE striking faults in the NW External Dinarides of Slovenia unravelled by mesoscale fault-slip data analysis. Geologia Croatica, 69(3), 295-305, 2016.

Živčić, M., Suhadolc, P. and Vaccari, F.: Seismic Zoning of Slovenia Based on Deterministic Hazard Computations. Pure appl. geophys. 157, 171-184, 2000.

840 Živčić, M., Čarman, M., Gosar, A., Jesenko, T. and Zupančič, P. Potresi ob idrijskem prelomu. In: Janež, J. (ed.). Anno domini 1511, (Idrijski razgledi, 2011, 1). Idrija: Mestni muzej., p. 119-126, 2011.